2009-01-0829

Compressive Neck Injury and its Relationship to Head Contact and Torso Motion during Vehicle Rollovers

James Raddin and Joseph Cormier
Biodynamic Research Corporation

Brian Smyth and Jeffrey Croteau
Exponent Failure Analysis Associates, Inc.

Eddie Cooper
B33 Consulting, Inc.

ABSTRACT

Previous literature has shown that serious neck injury can occur during rollover events, even for restrained occupants, when the occupant's head contacts the vehicle interior during a roof-to-ground impact or contacts the ground directly through an adjacent window opening. Confusion about the mechanism of these injuries can result when the event is viewed from an accelerated reference frame such as an onboard camera. Researchers generally agree that the neck is stressed as a result of relative motion between head and torso but disagree as to the origin of the neck loading.

This paper reviews the principles underlying the analysis of rollover impacts to establish a physical basis for understanding the source of disagreement and demonstrates the usefulness of physical testing to illustrate occupant impact dynamics. A series of rollover impacts has been performed using the Controlled Rollover Impact System (CRIS) with both production vehicles and vehicles with modified roof structures. Data from these tests were analyzed in both the vehicle reference frame and an inertial reference frame to demonstrate the neck injury mechanisms. The results of these tests show that neck loading was fundamentally a result of torso augmentation rather than roof deformation.

INTRODUCTION

The collection of publications in the literature on the role of roof structure deformation in occupant injury causation is extensive. Much of the early literature either treated the minimization of roof intrusion into the occupant space as implicitly desirable, or presented data which suggested that an association between roof crush and injury implied causation (Strother et al., 1984).

Initial studies of the General Motors testing series known colloquially as "Malibu" found that reinforced roof structures did not afford an increased level of protection for either restrained or unrestrained occupants when compared to production roofs (Bahling et al., 1990, Orlowski et al., 1985). These studies concluded that compressive neck loading at a magnitude associated with cervical spine injury is not caused by roof crush, but by the occupant moving toward the roof panel which is in contact with the ground, and that peak neck loads occur prior to significant roof deformation. A later study of a number of rollover tests in the literature, including the Malibu data, reaffirmed this conclusion (James et al., 1997). Occupant and vehicle motions in the Malibu tests have been further reexamined to quantify occupant and vehicle motions using techniques such as digitized film analysis, in which the occupants' heads were observed

The Engineering Meetings Board has approved this paper for publication. It has successfully completed SAE's peer review process under the supervision of the session organizer. This process requires a minimum of three (3) reviews by industry experts.

ISSN 0148-7191

to consistently reach the roof area prior to upper vehicle structure-to-ground impact (Gloeckner et al., 2007). A recent study used a computer simulation to demonstrate that when occupant head excursion is sufficient to contact the interior roof panel, compressive preloading of the neck can occur during the airborne phase of the rollover and prior to roof-to-ground contact, effectively reducing the dynamic loading required for injury on subsequent roof-to-ground impacts (Ashby et al., 2007).

The Controlled Rollover Impact System (CRIS) is a machine that was developed to produce a specific and repeatable rollover impact event, which does not impose any external constraints on the vehicle during or after the initial roof-to-ground impact. (Carter et al., 2002, Cooper et al., 2001). Recently, the CRIS has been used to compare production vehicle roof-to-ground impacts with corresponding impacts of vehicles modified with roll cages (Moffatt et al., 2003). This study reached conclusions similar to those in the Malibu work and found no significant difference in head accelerations and neck loads even when there was deformation of the production vehicle roof structure. These studies have consistently concluded that peak head accelerations and neck loads are the result of the roof striking the ground and stopping and the occupant "diving" into the roof, and are not caused by roof structure deformation.

In 2007, a study was published in light of proposed changes to FMVSS 216 related to rollover crashworthiness (James et al., 2007). In response to the methodologies employed by critics of the original Malibu findings, this study concluded that "observations from an inertial reference frame are necessary to correctly interpret the relationship of vehicle and occupant motions during a rollover crash". This study also found that neck loading is the result of the torso moving toward the head, and not roof intrusion that would cause the head to move toward the torso.

In 2005, an extensive overview of available literature on the topic of roof strength and occupant head excursion was published, outlining factors influencing overall head excursion and discussing a number of countermeasures and areas for expanded research (Moffatt and James, 2005).

Despite findings that dismiss roof deformation as the basis for compressive neck injury, the topic remains contentious. A study that analyzed high-speed Malibu test video and correlated injury to "roof intrusion rates", concluded that roof collapse in a rollover "imposes velocities and forces on an occupant's head that are far greater than an occupant would experience solely from his or her dropping at the vertical velocity of the vehicle's center of gravity" (Friedman and Nash, 2001). The same authors also concluded in a later reexamination of Malibu timing data that neck load is caused by roof intrusion "pushing" the head toward the torso (Friedman and Nash, 2005). The long time delays between A-pillar ground contact and peak neck loads, which were the basis of the authors' conclusion, were shown to be misinterpretations of the original Malibu work (James et al., 2007). Another study which reexamined Malibu data attempted to correlate the timing of peak "roof acceleration" to peak occupant neck loading (Chirwa et al., 2006). This study was shown to have confused vehicle body displacement with roof displacement with respect to the inertial reference frame, and failed to demonstrate a causal relationship between roof crush and neck loading (James et al., 2007). An examination of the timing of peak neck loads and roof crush in a series of Ford Explorer rollover tests concluded "roof crush into the survival space of restrained dummies was the direct cause of neck loads…" (Bidez et al., 2005). This study evaluated data in a vehicle-fixed rather than earth-fixed reference frame. Errors have been identified in this study's computation of instantaneous roof crush (Yamaguchi et al., 2007). Yamaguchi et al corrected the original derivations and found these methods of computing dynamic roof crush to be "theoretically feasible" but "completely impractical" due to current sensor technology limitations.

The purpose of this paper is to discuss rollover kinematics using fundamental principles and to demonstrate those principles using rollover test data.

ROLLOVER PRINCIPLES

The literature continues to include contradictory papers on the role of roof deformation in rollover neck injury primarily because there remain significant differences in the ways people understand the rollover event. Previous authors tend to portray rollovers either in qualitative terms that are technically deficient or in quantitative terms that are mathematically unapproachable for the average reader. The importance of distinguishing between body-fixed versus inertial reference frames is commonly neglected in the analysis of occupant dynamics in rollovers. This paper will first attempt to characterize the physical rollover event in approachable terms and then define and present data relevant to neck injury causation within that context.

The first requirement is to observe the rollover event from a non-accelerated, non-rotating reference frame, usually called an inertial reference frame. For our purposes, this can be a frame of reference fixed to the earth or moving at constant velocity. If this requirement is not met, motions of objects observed from an accelerated reference frame can be mistakenly ascribed to what are called “fictitious forces” (Serway, 1996). In other words, the accelerations of the reference frame result in what appear to be accelerations of some object of interest, and, therefore, forces on that object are imputed. In rollovers, this problem commonly arises in interpretation of film or video taken from a vehicle-mounted camera. Ground-based cameras are used to document the vehicle dynamics but vehicle-mounted cameras are more commonly used to study occupant motion. Authors may refer to an observed change in motion of an Anthropometric Test Device (ATD) when, in fact, the observed change in motion may result from a vehicle impact which has changed the motion of the vehicle-mounted camera. This error can cause attribution of injury to forces that are not there with resulting inappropriate protection recommendations.

A second requirement is to adequately describe the motion of the relevant parts of a vehicle involved in a rollover event. Mathematically, the motion of the center of mass as a function of time can be described with respect to an inertial reference frame. The motion is typically described using time functions of displacement, velocity and acceleration. For a rigid body, one can then define the motion of any other point in the body if the angular velocity is also known. For example, the velocity of a Point P in the body is defined by the following equation, where r is the distance from the center of mass to Point P and is the angular velocity in radians per second.

$$\vec{V}_P = \vec{V}_{cm} + \vec{\omega} \otimes \vec{r}$$

This general equation involves vector cross products and vector sums, but it is more approachable and illustrative if we reduce it to a simple, specific case.

Consider a symmetrical wheel rolling at constant velocity on a flat, horizontal surface, as shown in **Figure 1**.

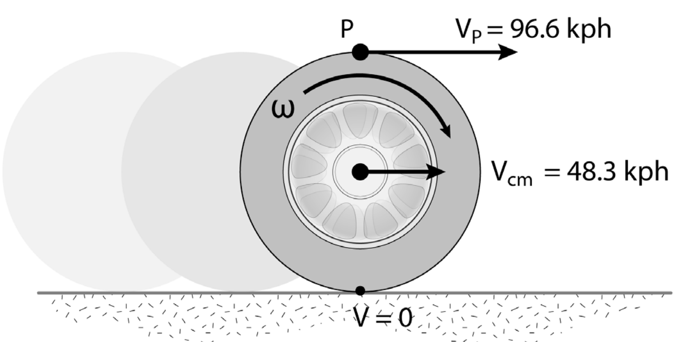

Figure 1: Wheel rolling at constant velocity.

The velocity of the wheel would be described as V_{cm} which would be entirely horizontal, say 48.3 kph or about 13.4 m/s with respect to an inertial or fixed reference frame. If the radius of the wheel is 1.07m and if there is no slipping of the wheel on the surface, we can compute the magnitude of the rotation rate with the following equation.

$$\omega = \frac{v}{r}$$

where ω is the rotation rate in radians per second, v is the velocity in meters per second, and r is the radius in meters. For our example, equates to about 12.5 radians per second or nearly 2 revolutions per second. If we were to calculate the velocity of a Point P on the edge of the wheel, again from a fixed reference frame, the observed instantaneous velocity would vary with time depending on where Point P happened to be. Its velocity is in the same direction as the center of mass at the top and in the opposite direction at the bottom. The resultant velocity would never be 48.3 kph in a horizontal direction. In fact, the velocity of Point P when it is right at the bottom would be exactly zero since the wheel is not slipping or moving against the surface. The velocity of P reaches a maximum in the horizontal direction when P is at the top and the vector sum of the velocity is twice the velocity of the wheel’s center of mass or about 96.6 kph. In accordance with the vector sum in the first equation, a point on the surface of the rolling wheel has a velocity that is the vector addition of the center of mass velocity and the tangential velocity. The tangential velocity has both magnitude and direction and while its magnitude remains constant (for a constant center of mass speed) the direction of the tangential velocity varies with time. The velocity of P for three distinct wheel orientations is shown in **Figure 2**. The velocity of P, in terms of its horizontal and vertical components, takes the form of trigonometric functions and is shown in **Figure 3**.

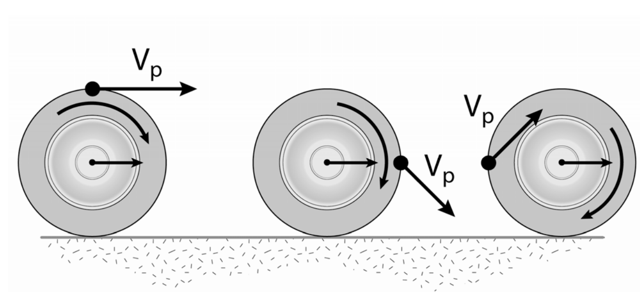

Figure 2: Resultant velocity of point on rolling and translating wheel.

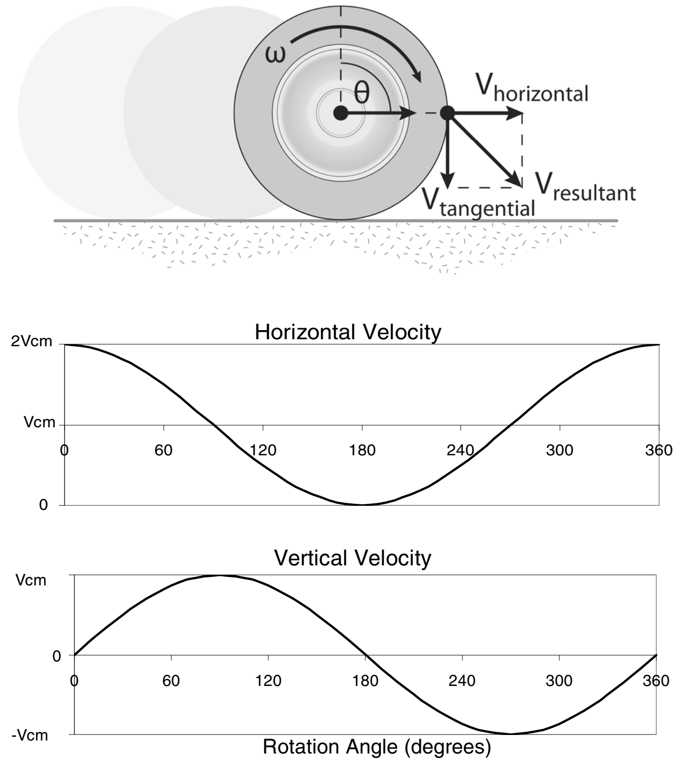

Figure 3: Horizontal and vertical velocity components of point P for one revolution.

The third law of motion states that for every force there is an equal and opposite reaction force. The second law dictates that the sum of the forces gives rise to the rate of change of linear momentum. For our wheel, there is a constant force being applied by the spokes that acts at a 90º angle to the tangential velocity of point P to change its direction but not its magnitude. This is termed a centripetal force and produces a centripetal acceleration in accordance with the second law of motion. A freely movable bead on a spoke of our wheel would move radially outward to the rim until a force constrains it within the wheel's path. This bead motion is analogous to what happens to occupants in rolling vehicles. The inertial force that moves the bead out to the periphery is called a centrifugal force and is equal and opposite to the force of the bead as it loads the wheel rim. In vehicle rollovers, every point in the vehicle and in the occupants generally has a different instantaneous velocity, acceleration, and force taking place. The inertial centrifugal force is directly proportional to both radius and the square of the angular velocity, always directed along a radius from the center of mass. As measured at the head, this force may exceed ten times the force of gravity in a high-speed rollover (for a 550 deg/s roll rate and a 1.07m radius).

A final observation with our wheel analogy relates to angular momentum and angular energy which are angular analogs of the more familiar concepts of translational momentum and energy. For the translational case, we have

$$\text{Momentum} = \vec{P} = m\vec{v}$$

$$\text{Translational Energy} = E_T = \tfrac{1}{2}mv^2$$

where momentum is a vector quantity (having both direction and magnitude) and energy is a scalar. The mass of an object is a measure of its resistance to being accelerated by a force. The angular analog is called moment of inertia (I), which is a measure of an object's resistance to being spun around a specific rotation axis by a torque or twisting force. We therefore have

$$\text{Angular Momentum} = \vec{L} = I\vec{\omega}$$

$$\text{Angular Energy} = E_A = \tfrac{1}{2}I\omega^2$$

Just as momentum is changed by a force acting over time (impulse) and energy is changed by a force applied over distance (work), angular momentum is changed by torque over time and rotational energy is changed by torque acting through an angle. It should be noted that angular momentum and translational momentum have different units (torque-time vs. force-time) while translational and angular energies share the same units (force-distance). The practical application of these concepts includes the understanding of how angular energy and translational energy interchange in a rollover. Specifically, a sliding vehicle prior to rollover has virtually all its energy in a translational form. When it is rolling, some of that energy is converted to angular energy, which implies that it has less translational energy and, therefore, a lower velocity of the center of mass. In other words, when a vehicle starts rolling, its over-the-ground velocity slows down. The proportion of the original translational energy temporarily transformed into rotational energy may be in the range of 10% to 25% or more. The angular momentum of the rolling vehicle also imparts gyroscopic characteristics which result in precession and nutation effects. These are rarely taken into account in rollover analyses but would rationalize what is more commonly assessed to be a chaotic process.

Vehicles typically do not roll like wheels or barrels, but the same mathematics apply. Among the differences is the typical lack of the non-slip situation described above. The external influence that makes vehicles roll is the interactive force between the exterior of the vehicle and the terrain. That force tends to get less effective in increasing the roll rate as the magnitude of the tangential velocity approaches the center of mass velocity. Therefore, the tangential velocity is usually lesser in magnitude than the center of mass velocity. This means that the horizontal component of the velocity of a part of a rolling vehicle in contact with the ground is generally less than the center of mass velocity but more than zero as would have been the case with a wheel. The vehicle-ground interaction induces a torque into the vehicle that results in scrapes left on the vehicle. The scrapes can typically be used to assess the roll direction since they are formed in the direction of the angular rotation, or down on the leading side and up on the trailing side, as shown in **Figure 4**.

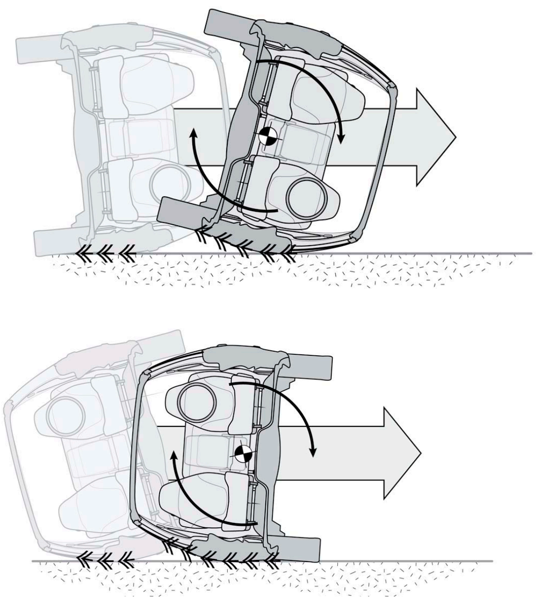

Figure 4: Direction of scrapes created by the vehicle-to-ground interaction.

The velocity of a part of the vehicle away from the ground (and above the center of mass) will be more than that of the center of mass velocity but generally less than twice as much as it would have been in the case of the wheel example presented in **Figure 3**. This explains why occupants ejected from the high side in a rollover leave the vehicle with a higher velocity than those ejected from the low side.

The conceptual underpinnings have now been reviewed sufficiently to allow an examination of the ground impacts of a rolling vehicle. Consider another symmetrical wheel rotating with a constant horizontal velocity but supported barely above a horizontal surface. It is then allowed to touch down on the surface with negligible vertical velocity while rotating at an angular velocity lower than that necessary to roll without slip on the surface. The touchdown will result in a frictional force between the surface and the wheel that will tend to accelerate the angular velocity of the wheel by acting as a torque, as shown in **Figure 5**. The torque in this case produces an angular acceleration that changes the angular velocity in direct proportion to the torque and in inverse proportion to the moment of inertia.

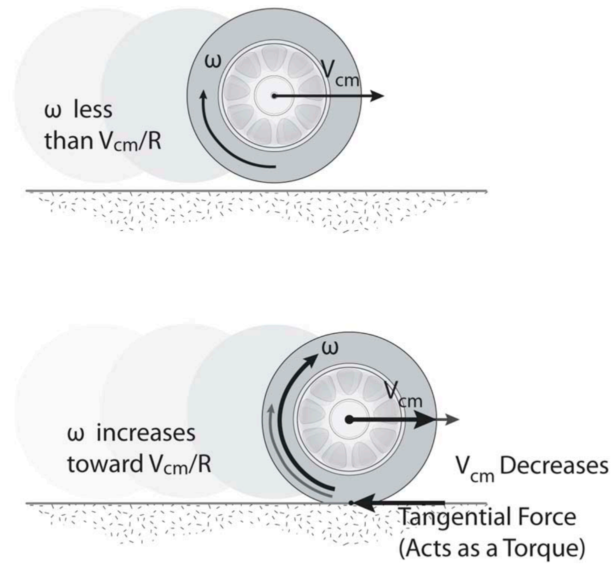

Figure 5: **Increase in rotational velocity with touchdown of horizontally translating wheel.**

If we were to drop the same wheel from a greater height, it would arrive at the surface with a vertical velocity as well as a horizontal one. Force would be applied by the surface to the wheel (and equally and oppositely by the wheel to the surface) that would be more complex. As shown in **Figure 6**, there would be a vertical (or normal) component of force acting through the center of mass of the wheel to reduce the downward velocity of the wheel.

There would again be a horizontal (or tangential) component acting at a 90º angle to the radius acting as a torque to increase the angular velocity of the wheel similar to the previous example. In general, the coefficient of restitution during the impact will insure some degree of bounce since the normal force not only slows the vertical velocity to zero but also typically continues to act to impart a vertical velocity upward as the elastic compression of the wheel is reversed.

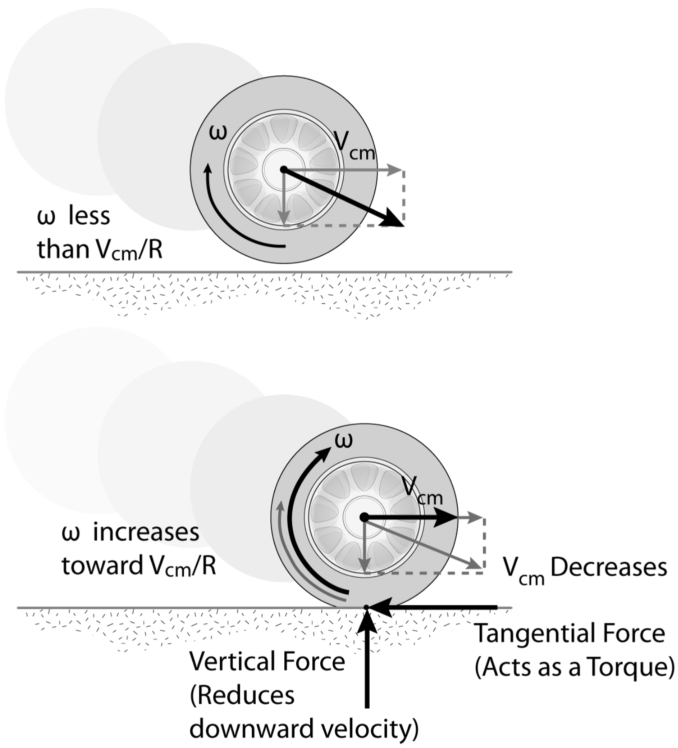

Figure 6: Force generated by touchdown of vertically and horizontally translating wheel.

Vehicle-ground interaction is further complicated by vehicle shape. The roof rail is generally further from the center of rotation, for example, than the center of the roof. The roof rail will generally not contact the ground just as the radius from the center of rotation to the roof rail passes through vertical. When it doesn't, the vertical force from the ground will also tend to act to some extent as a torque, as shown in **Figure 7**, and the horizontal force will also tend to act to a greater extent on the center of mass. Note that **Figure 7** only shows the effect of the vertical component which becomes predominant as increases toward V_{CM}/R and as the vertical component of V_{CM} increases.

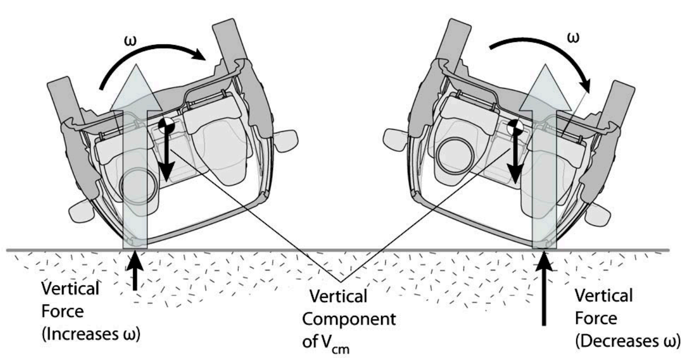

Figure 7: Effect of vertical component of contact force on rotation.

In general, vehicle-to-ground contact may increase or decrease the angular velocity depending on the interaction. Some contacts may first decrease and later increase the angular velocity during a single contact with the net effect depending on the comparative contributions. The graphic in **Figure 7** shows a near-side contact followed by a far-side contact. The continued rolling of the vehicle in this configuration requires some combination of deformation or rapid change of the vertical velocity of the center of mass of the vehicle. There is simply no room for the undeformed far-side roof rail to miss the ground given the downward moving center of mass and the radius to the roof rail being greater than the distance from the center of mass to the ground. This is the reason that designers reject the use of square shapes as wheels and explains why trailing roof rails are often rounded off by rollover deformation. It is fundamentally the same conceptual reason that an occupant whose head is already against a trailing roof rail at a far-side ground contact will be exposed to neck loading prior to roof deformation.

Another effect of irregular vehicle shape is that the tangential velocity of the contact point will in general affect the vertical velocity of the contact, as shown in **Figure 8**. The vertical contact velocity of the roof rail without rotation would simply be the vertical velocity of the center of mass, or 8.05 kph in the example shown in **Figure 8**. With rotation, the roof rail contact velocity will be the vector sum of the center of mass velocity and the tangential velocity at the roof rail. In our example, the vertical velocity of the roof rail contact would increase to 20.45 kph and the horizontal velocity would decrease to 6.28 kph. This increased vertical velocity is certainly within an injurious range, independent of roof deformation. Inverted drop tests conducted with vehicles and instrumented ATDs released from 0.46m that achieved contact velocities of 10.8 kph have been shown to result in injurious neck loads (Nightingale, 1996). Contact of the trailing side roof rail with terrain before it passes under the center of mass is again the most hazardous condition for producing increased vertical velocities.

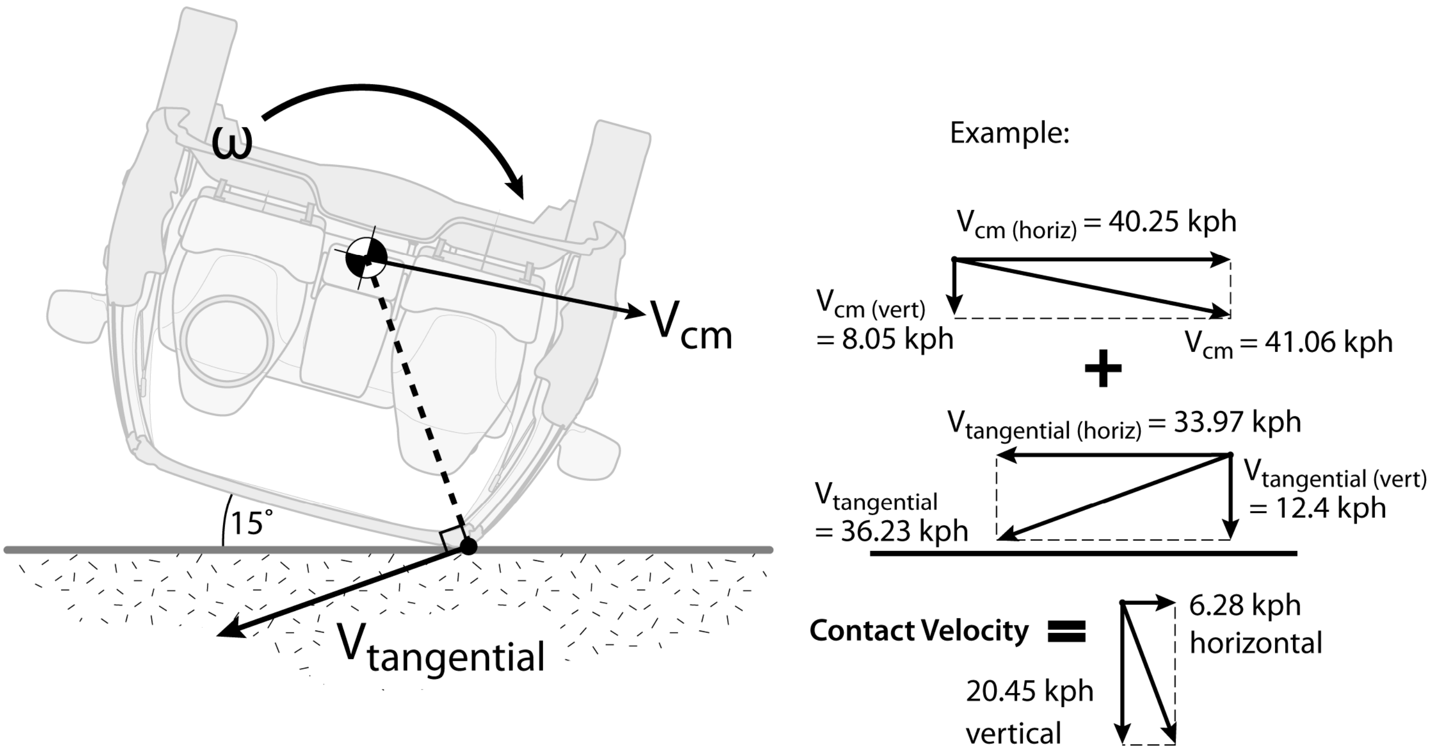

Figure 8: Influence of vehicle rotation rate on contact velocity at roof contact.

Vehicle deformation introduces yet another complexity, as all real materials deform. An idealized non-deforming vehicle bouncing and rolling on a non-deforming surface would experience infinite forces and accelerations. The relatively modest accelerations measured at the center of mass of a rolling vehicle attest to the attenuation (cushioning) effect that the deforming structures make when contacting the ground. The deformation lengthens the distance and duration of the impact, decreasing the peak translational acceleration of the center of mass and of the non-contacted portions of the vehicle. Accelerations of parts of the vehicle nearer the contact point are much higher (Carter et al., 2002). Increased roof stiffness would increase the center of mass acceleration at roof contact and, therefore, increase relative occupant displacements. Further increases in contact severity occur with terrain variations such as an impact into rising terrain, since more of the vehicle horizontal velocity acts like an increased vertical velocity.

The increased time of the contact results in another important effect. Ground contacts in rollovers where the vehicle has high translational and angular velocity may have durations in the range of 100-200 milliseconds. The very late contacts may last even longer. Therefore, the force from the terrain acts at a changing angle during the contact, which often changes over an angular range of more than 40 to 60 degrees as the vehicle continues to rotate and translate and the contact point continues to slide.

Occupant kinematics within the vehicle will vary depending on how the vehicle strikes the ground. For a rolling vehicle, the occupant does not simply move toward the point of ground contact but rather responds in accordance with the laws of motion, generally in a curving path with respect to the rotating vehicle. The centripetal effects at the vehicle periphery ensure the occupant's head is not at a neutral driving position during most of a multi-rollover event. Instead, it is typically at or near the roof rail, which is reachable by most restrained adult occupants since it is generally lower than the roof above a neutral head position. After window breakage, the head may pass beyond the roof rail, becoming susceptible to direct terrain contact. Vehicle-to-ground impacts during a roll sequence can affect occupant kinematics such that head-to-vehicle contact also occurs inboard of the roof rail. The most hazardous impacts typically occur when a trailing side roof rail hits the ground because the tangential velocity is more likely to add to vertical contact severity on the trailing side and decrease vertical contact severity on the leading side. At contact, direct roof rail loading of the head may occur as the roof or roof rail undergoes a significant change in velocity with the head already against it. For typical trailing side roof rail contacts, occupant head motion may carry on out the window since the occupant does not simply move toward the roof rail in contact with the ground.

The complex motions described above dictate the type of test approaches required to investigate them. Simple inverted drop tests are a poor comparison for the following reasons. The lack of vehicle angular velocity mispositions the occupant vertically and laterally since there is no centrifugal or centripetal force. In fact, even the displacing effect of gravity is lost once the vehicle is released. Secondly, the vehicle structure is loaded unrealistically since there is no horizontal component of contact force and no changing angle of force. Thirdly, the occupant kinematic response is not representative since the occupant has only a vertical velocity and it is not subjected to the angular rotation effects. Finally, reference frame confusion is often introduced through the use of vehicle-mounted cameras. Drops onto a roof rail are similarly not representative of the conditions in a roof-to-ground impact during a rollover.

Other test approaches have been devised with rotating vehicles and moving impact surfaces (Friedman et al., 2007) that have more intuitive appeal and may be repeatable but that repeatedly involve fundamental problems. Most critically, the dynamics of these devices lead to the imposition of unrealistic impact forces derived from the constraints imposed by the fixture. They do not have six degrees of freedom like a rolling vehicle, so unrealistic impact forces result from the way the vehicle is prevented from moving along and about the constrained axes. The problems are compounded when partial vehicle segments are used. These are typically weight compensated but the moments of inertia are not representative, resulting in both the rotational and translational impact dynamics being wrong. Finally, reference frame problems are introduced if changes in the velocities of the moving impact surface and the dropping vehicle are unrepresentative of a real impact, no matter where you mount the cameras. To achieve representative impact loading on the vehicle and on the occupant, a true six degree-of-freedom or unconstrained impact must be employed.

It is important to get the mechanism of neck loading right. Otherwise, incorrect notions may lead to well-intentioned interventions with unanticipated adverse effects. For example, attempts to increase the strength of roof supports typically result in more elastic structures that have greater elastic recovery (or bounce more). This results in increased velocity changes for roof-to-ground contacts, increasing the energy change of the event not only for occupants against structure at the contact location but also for remotely located occupants.

ROLLOVER TESTING

To assist in understanding the source of neck loading in rollover impacts, a compilation of test data was reviewed from tests in which impacts were produced, which involve all the rotational, translational, gravitational, and impact conditions of an unconstrained rollover ground impact.

Data were assessed from an inertial frame of reference by utilizing inertial sensors in the head of the ATD. The inertial sensors or accelerometers inherently measure with respect to an inertial reference frame. At the same time, neck load cells measure real forces so that reference frame confusion can be avoided. If, as some authors have claimed, injurious neck force is derived from the head being accelerated into the neck by roof deformation, then the inertial sensors in the head should measure significant acceleration as the roof deforms and the neck is loaded. If, on the other hand, the inertial sensors do not measure significant acceleration of the head during neck loading or during roof deformation, then the neck forces must derive from some other source such as torso loading, or torso augmentation. In particular, contacts of reinforced vehicles with little roof deformation should yield negligible neck loads if neck loads are the result of roof deformation.

CONTROLLED ROLLOVER IMPACT SYSTEM

The Controlled Rollover Impact System (CRIS) is currently the only system that can repeatedly orient a full vehicle for a specific impact while allowing six degrees of freedom (**Figure 9**). The ability to repeatedly configure a specific impact allows direct comparison between production and reinforced roof structures.

Figure 9: Photograph of CRIS system with vehicle attached.

The CRIS consists of a Class-8 tractor and a flatbed trailer that has been modified so that a full-size vehicle can be hung from adjustable supports at the back of the trailer. The vehicle can be spun about its principal roll axis with bearings that are located at the front and rear of the test vehicle. While the test vehicle's principal axis is fixed relative to the vehicle, this axis can be adjusted relative to the ground. This adjustment allows the test vehicle to be configured to a specific pitch angle, yaw angle, and drop height. Vehicle translation speed is determined by the speed of the tractor-trailer.

An electric motor spins the test vehicle up to the desired roll rate, and the front and back of the vehicle is released simultaneously at both ends. The release is timed so that the vehicle is at the intended roll angle when it impacts the ground. Once the test vehicle is released from the CRIS it is unconstrained, and, therefore, it has six degrees of freedom at impact.

ROLLOVER TEST DATA

Data from ten CRIS tests were analyzed where Hybrid-III ATDs were restrained in the driver seating position of the test vehicles. The tests were conducted to simulate a passenger-side leading rollover with a roof-to-ground impact on the driver side roof. This configuration is also referred to as a far-side occupant impact. A secondary impact was analyzed for the Isuzu Rodeo test where the ATD's head directly contacted the ground through the adjacent window opening (**Figure 10**). By design, except for the second Rodeo impact, all ATD impacts occurred near the 180-degree roll angle. The Volvo XC90 had a pitch angle of 5 degrees at impact, while all other test vehicles had a zero pitch and yaw angle at impact. Refer to **Table 1** for a summary of each impact configuration.

Figure 10: Onboard video showing the head-to-ground contact during the second impact in the Rodeo CRIS test.

Table 1: CRIS test initial conditions at roof contact: translational speed, drop height, and roll rate.

Vehicle	[kph]	[cm]	[deg/s]	ATD	Roof
2005 Volvo XC90	12	27	224	50th	Prod.
1996 Isuzu Rodeo 1	60	48	317	5th	Mod.
1996 Isuzu Rodeo 2	--	--	--	5th	Mod.
1998 Ford Crown Victoria	13	27	227	50th	Mod.
1999 Ford Crown Victoria	13	27	226	50th	Mod.
1999 Ford Crown Victoria	13	28	223	50th	Prod.
1998 Ford Crown Victoria	13	30	227	50th	Prod.
2000 Ford Crown Victoria	32	33	363	50th	Mod.
1999 Ford Crown Victoria	32	32	361	50th	Prod.
1996 Chevrolet Blazer	13	25	226	50th	Prod.
1996 Chevrolet Blazer	13	25	226	50th	Mod.

Instrumentation for the CRIS tests included test vehicle roll rate at release, test vehicle translation speed at release, ATD triaxial head accelerations, and ATD upper-neck triaxial forces and moments. A detailed analysis was conducted on the data collected during these tests. The data referenced to the vehicle coordinate system will be presented in standard SAE J211 sign convention; i.e. the positive longitudinal axis is forward, the positive lateral axis is to the right, and the positive vertical axis is down.

The inertial reference system will be defined with respect to earth with the positive lateral direction oriented by the travel direction of the CRIS test device (**Figure 11**). The longitudinal and vertical directions will be defined from the lateral axis using the right hand rule; i.e. the positive longitudinal axis oriented generally in the vehicle longitudinal direction, and the positive vertical axis into the ground. Note that the positive vertical axis for both the vehicle and earth reference frame are collinear when the vehicle is at a 0-degree roll angle.

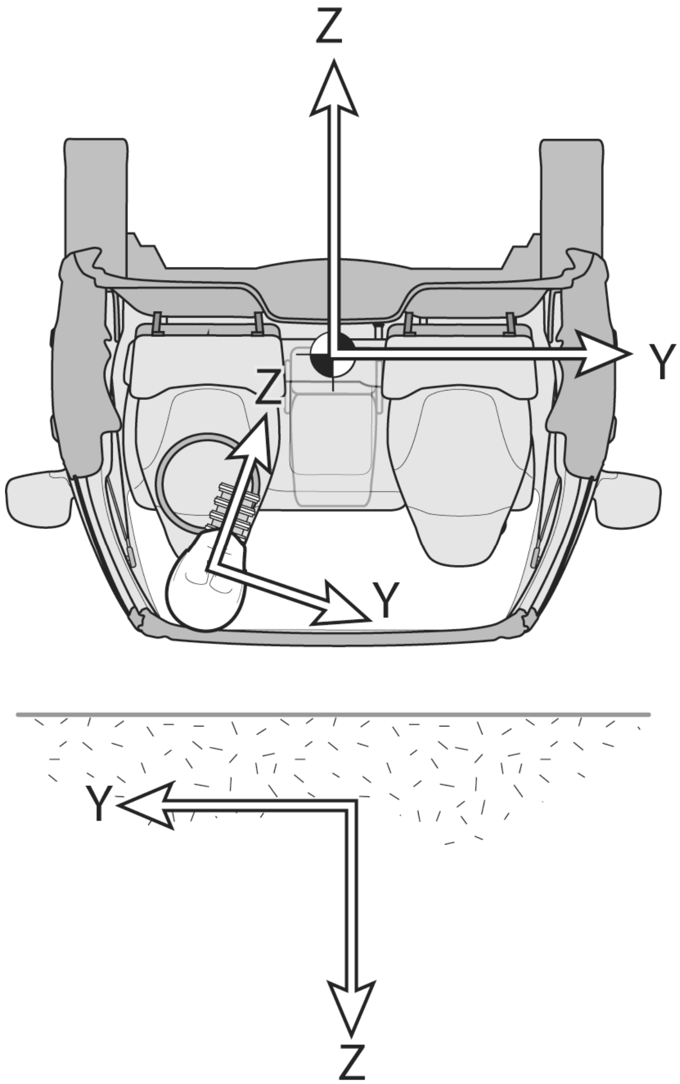

Figure 11: Vehicle, head and inertial coordinate systems.

ATD data were collected according to standard SAE J211 sign conventions. Head accelerations are positive in the longitudinal direction with a forward acceleration, in the lateral direction with a rightward acceleration, and in the vertical direction with a downward acceleration. The ATD upper neck positive signals are consistent with the reaction forces from the head acting on the upper neck. Therefore, a positive upper neck longitudinal force is consistent with an aft force applied to the front of the head, a positive lateral force is consistent with a lateral force applied to the right side of the head, and a positive vertical force is consistent with a tension force applied to the top of the head, resulting in a left hand reaction coordinate system.

The authors suggest that analysts carefully conduct this type of analysis and should pay particular attention to the coordinate system in which the analysis is performed. Although ATD head accelerometers are oriented with the ATD's coordinate system, they inherently measure accelerations of the object to which they are attached within the inertial reference system. Therefore, accelerometer data from the ATD head cannot be directly used to determine accelerations at other points within the vehicle coordinate system, or the vehicle coordinate system itself. Comparison between inertial accelerations of the ATD head and the vehicle can only be done if inertial accelerations are known at another point of interest.

Information regarding the origin of ATD upper neck loads can be gleaned by using inertial accelerometer data from the ATD head to calculate forces at the head based on its mass, and then comparing these forces to those recorded at the ATD upper-neck. The total force applied by the ATD at the top of its head can be computed by summing the upper neck load and the calculated inertial head force as shown in the free body diagram of the head in **Figure 12** and represented by the equation below.

$$\text{Total head force} = -\left(F_{neck} + m^* a_{head} \right)$$

The force at the base of the head ($-F_{neck}$) is directly measured from the upper-neck load cell. The polarity of the neck load data will be inverted since we want it to represent the force of the neck acting on the head (earth coordinate system), which is opposite the SAE J211 sign convention. The measured neck force at this location includes the inertial forces reacted through the neck required to decelerate the torso, reducing its velocity component toward the ground.

The inertial head force can be calculated using Newton's second law of motion.

$$F = ma$$

The head mass is based on information specific to the ATD, and its acceleration was measured at its center of gravity throughout the event. Like the neck load data, the measured head accelerations are inverted since the free-body diagram is represented in the earth coordinate system, and the force of the head is acting in the opposite direction of the recorded accelerometer data. The lateral components of these forces were also analyzed in a similar manner.

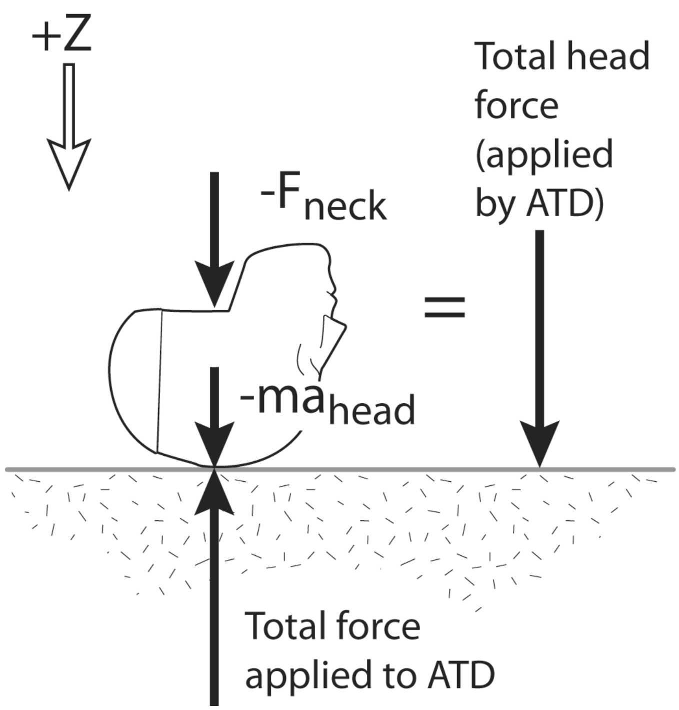

Figure 12: Free-body diagram of vertical head forces.

Although the head accelerometers measure accelerations in an inertial reference frame, they do so at an orientation consistent with the ATD head. Calculating the forces in an inertial reference frame consistent with the earth coordinate system defined previously will require a coordinate transformation. This is also true for the vehicle coordinate system. The effects of these transformations depend on head angle, vehicle angle, and the relative magnitudes between the vertical and lateral components of acceleration. If the head angle is small relative to the coordinate system of interest, then the difference between calculations in the head coordinate system and the coordinate system of interest will be small. This is especially true if the components of force in directions orthogonal to the direction of interest are small when compared to the direction of interest.

Effects of head and vehicle angle on this analysis were considered for selected impacts. Video analysis from one of the onboard high-speed video cameras was used to determine the ATD head angle relative to the vehicle reference frame. Head and roof displacements were also determined from video analysis of the onboard camera. Additional video analysis was performed from cameras onboard the CRIS fixture, and from ground-based cameras. Data from these cameras included head displacements and vehicle roll angle. Low frequency video data was curve-fit using polynomial functions to estimate positions between points measured at each video frame.

Video data can be used to assess overall motion of the ATD head within the reference frame in which it is recorded. However, since the video acquisition rate of the high-speed cameras was 250 Hertz, time resolution of the video data is coarse compared to the neck load data at 10 kHz. The video can be used to define the initial conditions, the vehicle angle, and the head angle throughout the impact and then superimposed with the 10 kHz neck load data to illustrate the origin of the ATD upper-neck loads.

RESULTS

An analysis of the vertical head forces was conducted on the eleven head impacts from the CRIS tests presented in **Table 1**. The time history plots of the ATD data for each of the impacts from the CRIS tests can be found in the APPENDIX. In the next two sections, data collected from the production Volvo XC90 and the reinforced Isuzu Rodeo vehicles tested on the CRIS will be presented in detail. The load data from the instrumented ATD head, which is presented in the inertial reference frame (earth coordinate system), will be addressed first. It is followed by the presentation and discussion of the video analysis performed from the onboard cameras. The data is compared and contrasted to highlight the meaning of the results from analysis in each of the two coordinate systems.

VOLVO XC90 CRIS TEST

A production 2005 Volvo XC90 was dynamically balanced and tested on the CRIS machine. The initial conditions at impact were: 12.3 kph horizontal speed, 182 degree roll angle, 224 deg/s roll rate, 5 degree pitch, and zero yaw. The drop height, from release to first contact, was 274 mm. Prior to the test, the driver ATD had a head clearance with the interior of the roof panel of 38 mm in a static 1g inverted position; dynamically the head clearance would be less. The vehicle was released from the CRIS fixture, fell to the ground without any external constraints on the vehicle, and impacted the ground, as shown in **Figure 13**.

Figure 13: Ground contact with the exterior roof panel in the XC90 CRIS test.

The two plots in **Figure 14** and **Figure 15** represent the lateral and vertical component forces acting on the ATD head in the earth's inertial reference frame. The roof first contacted the ground at time T=0s, and occurred at the roof panel over the B-pillar. The blue traces represent the inertial head force obtained by multiplying only the head mass by the acceleration of the head in the respective directions. The orange traces represent the algebraic sum of the inertial head force and the measured neck load, transformed from the ATD reference frame to the inertial reference frame. The measured neck load is not shown separately in these plots for clarity, but it is presented in the head-based coordinate system in the APPENDIX. Observe that in the earth-based coordinate system (**Figure 12**) the vertical force from the head during a ground impact would be a positive quantity, as shown in the plot of **Figure 15**.

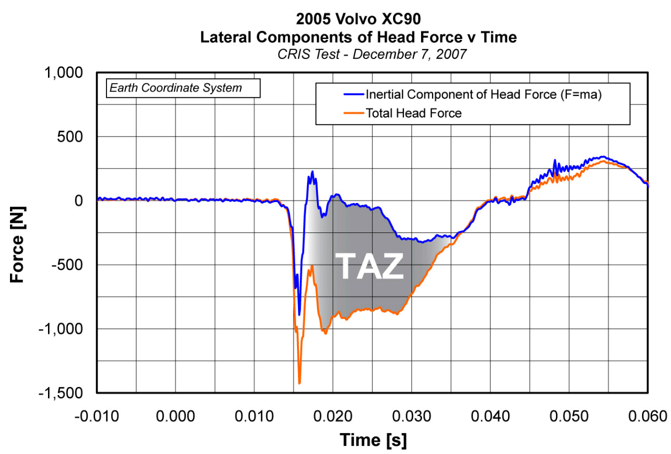

Figure 14: Lateral inertial and total head force during the XC90 CRIS impact.

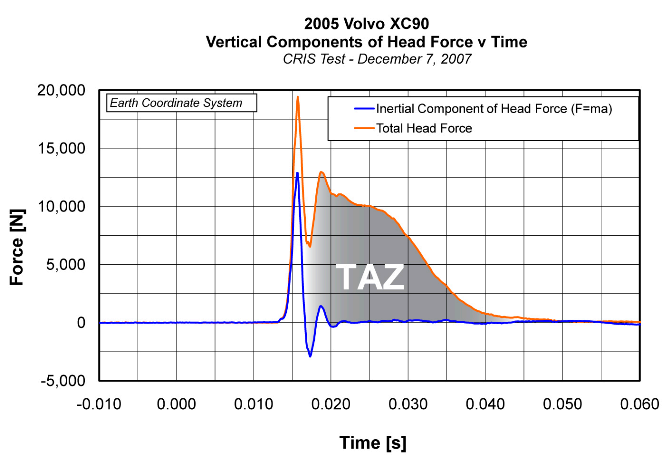

Figure 15: Vertical inertial and total head force during the XC90 CRIS impact.

The inertial head force, which by definition is governed by its acceleration, is generated by changing the velocity of the head within the inertial reference frame. Therefore, no inertial force is generated if the head remains at a constant velocity, or if the head has come to a stop. This is clearly shown in the data of **Figure 15** (blue trace) at the time prior to roof contact and after the transient response from the head deceleration after it struck the ground.

The total head force is dominated initially by the short transient response of the inertial component of the head force, which occurs within approximately 4 ms of the initial head contact (see **Figure 15**). This short duration force is the inertial component generated from changing the velocity of the head. When the inertial head force goes to zero, then by definition the head is no longer being accelerated; the vertical motion of the head is stopped against the ground but the head continues to move in the lateral direction. The later duration of the total head force represents the inertial force of the torso into the head through the neck, and is directly measured by the neck load cell. The effect of this inertial torso loading is what dominates the total head force after the inertial head force has diminished and is illustrated in the data of **Figure 14** and **Figure 15** as the Torso Augmentation Zone (TAZ).

The components of the head velocities and displacements were calculated from the accelerometer data in the earth reference frame. The components of the ATD neck load data were also transformed to the earth reference frame. Plots of the neck load data and the head displacement data are presented in **Figure 16**. The correlation of the earth-based head displacement and neck load data show the head is moving toward the ground (vertical direction) and stops at approximately 16 ms. This would indicate that it took 16 ms for the head to travel from its initial position to the roof panel, and for the roof panel above the ATD head to contact the ground. During the time that the top of the head is decelerating, there is simultaneous loading to the neck from the torso, which is measured by the neck load cell. The data clearly show that the head is not displaced into the torso when the peak neck load occurs. In fact, the vertical and lateral head displacements do not change appreciably over the duration where there is significant neck load.

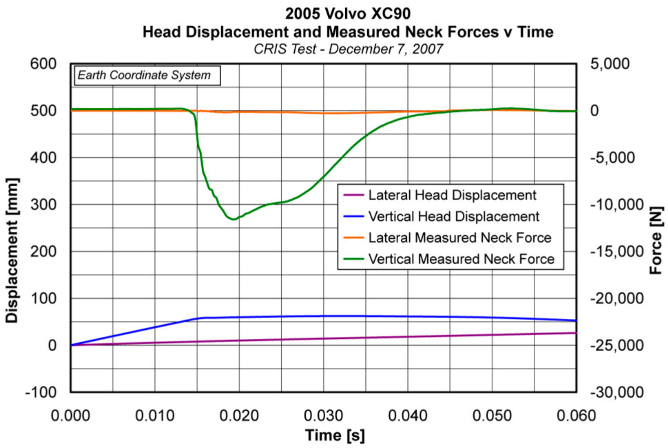

Figure 16: Measured neck loads and head displacements in the earth coordinate system.

The head velocities are correlated in time with the measured neck forces in **Figure 17**. The initial velocity from contact to the beginning of the inertial head loading is relatively constant at approximately 14 kph (note the linear displacement profile in **Figure 16**) and then abruptly experiences the change in velocity shown in **Figure 17**. Observe that the data also show that after approximately 16 ms the measured neck force only includes the force imparted on the head from the deceleration of the torso. Notice also that the vertical velocity of the head is zero because it is stopped against the ground during the time that the torso loads the neck.

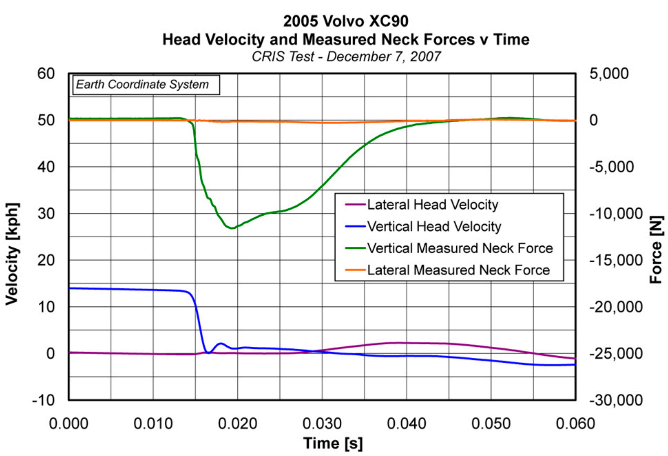

Figure 17: Measured neck loads and head velocities in the earth coordinate system.

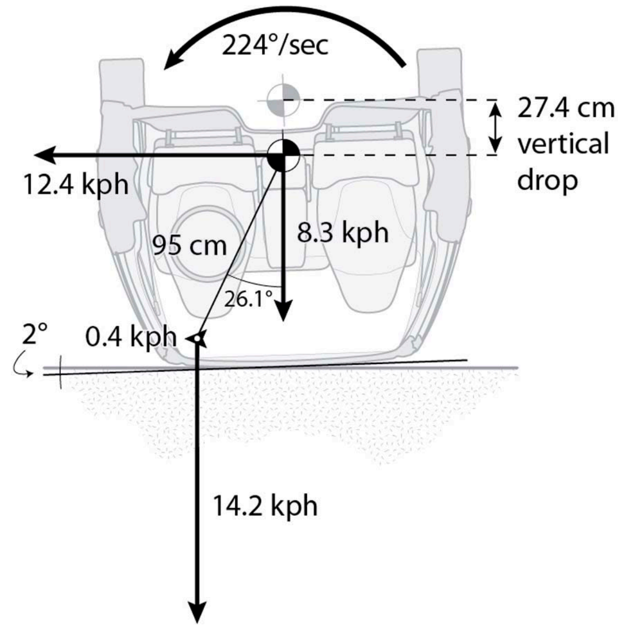

Figure 18: Vector velocity analysis of the XC90 impact in the earth-based reference frame (forward looking aft).

The initial vertical velocity data are compared in **Figure** 17 to a vector analysis using the initial impact conditions (**Figure 18**) showing that the change in head velocity compares quite well with the electronic data. The comparison confirms the validity of the analysis in the earth based inertial coordinate system as an appropriate means of assessing the injurious neck loading in this type of impact.

At vehicle contact with the ground during the XC90 test, the ATD head was just inboard of the left roof rail, as shown in **Figure 19**, which also shows the clearance between the ATD head and the interior roof panel.

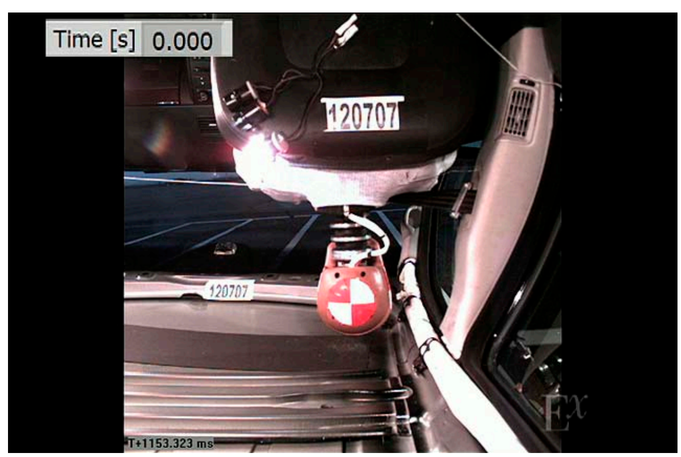

Figure 19: Screen capture of the onboard high-speed video of the driver ATD in the XC90 CRIS test at vehicle-to-ground contact.

The peak measured compressive neck load occurred at 19.3 ms and the nearest frame in the high-speed video to this peak was at 20 ms, which is shown in **Figure 20**. Observe the compression in the neck by comparing the aluminum neck rings at 20 ms versus the neck rings at the unloaded neck at 0 ms. Also observe that there is wrinkling of the roof panel at the time of this peak measured neck load. The magnitude of this roof displacement was evaluated by conducting a quantitative video analysis of the onboard high-speed video of the rear of the ATD in the vehicle based coordinate system. The apparent roof displacement and velocity were determined using on-board cameras with positive values indicating downward motion with respect to an upright vehicle.

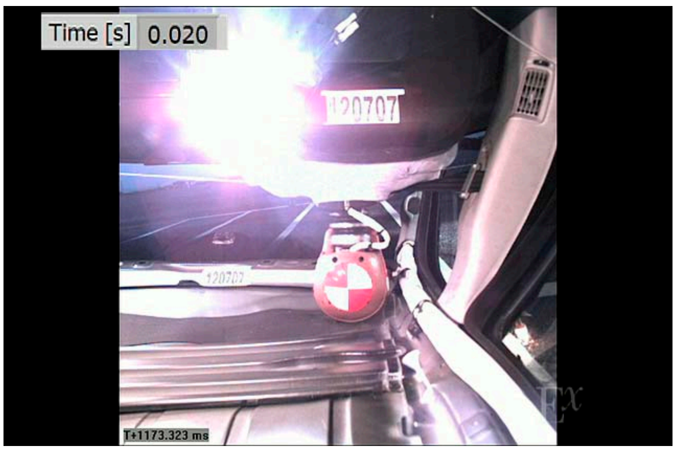

Figure 20: Screen capture of the onboard high-speed video of the driver ATD in the XC90 CRIS test near peak measured compressive neck load.

The video analysis data from the onboard camera revealed a negligible amount of head rotation during the compressive neck loading event. The roof and head displacements and velocities, both the lateral and vertical components, and the head angle were determined for the neck loading event. The vertical component of the head and roof displacements from the video analysis are plotted for the duration of the roof contact in **Figure 21**. The high-speed camera is mounted to the vehicle floor pan, which is undeformed during the roof-to-ground impact. As the roof contacts the ground, the roof stops vertically, yet the vehicle floor pan and the ATD continue to move toward the ground. When the high-speed video is analyzed from the accelerated reference frame (vehicle floor pan in this case), there is a quantifiable displacement of the head and roof relative to the camera. One must exercise caution in the interpretation of this data and realize that the displacement quantified by the plot is relative to an accelerated reference frame. The measurements are actually representative of the camera motion relative to the head and roof.

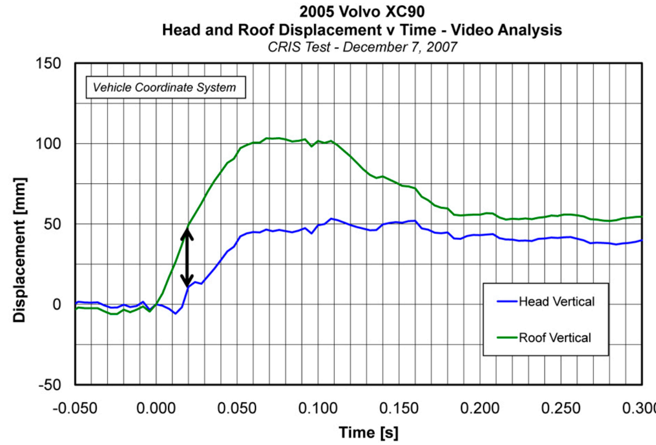

Figure 21: Apparent roof and head displacement calculated from the on-board high-speed video camera, which is attached to an accelerated reference frame.

The actual peak in the neck load occurred at 19.3 ms, which is depicted with the black double-sided arrow located two lines after time 0.000 s in **Figure 21**. This means that in the vertical direction, the camera moved 49 mm closer to the roof and 11 mm closer to the head during the time from contact to the peak neck load. The roof and head data from this accelerated reference frame video analysis show that the ATD moved (with the video camera mounted to the vehicle) toward the ground by 38 mm. This distance was the approximate clearance between the head and the roof panel. At peak neck load, therefore, the head was not affected by roof deformation.

A temporal comparison of the roof lateral and vertical velocities reveals a biphasic event. The vertical velocity peaks first at 76 ms and the lateral velocity peaks later at 88 ms. The phasing of these measurements is consistent with the roll angle at impact with the ground, i.e. adjacent to the ½ roll position. Note that the vertical velocity calculated in the accelerated reference frame was less than 10 kph, where in the inertial reference frame it was 14 kph.

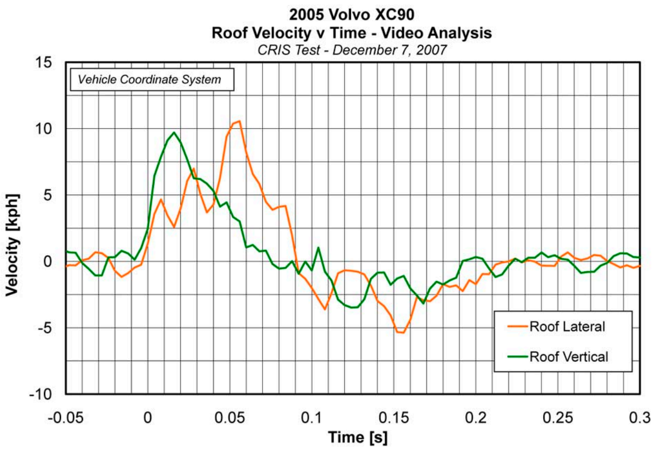

Figure 22: Apparent roof velocity calculated from the on-board high-speed video camera, which is attached to an accelerated reference frame.

Video analysis was also conducted in the inertial reference frame to demonstrate consistency with the earth-based analysis performed using the acceleration and neck load data recorded by the ATD instrumentation. This video analysis was conducted in the inertial reference frame from a camera attached to the CRIS fixture (see **Figure 13**). The ground was also tracked near the point of impact and used to remove any motion of the camera caused by the moving CRIS device. This ensured that the fixture-mounted camera was resolved in the earth reference frame. The components of the head displacements and velocities during the duration of head contact are illustrated in **Figure 23** and **Figure 24.**

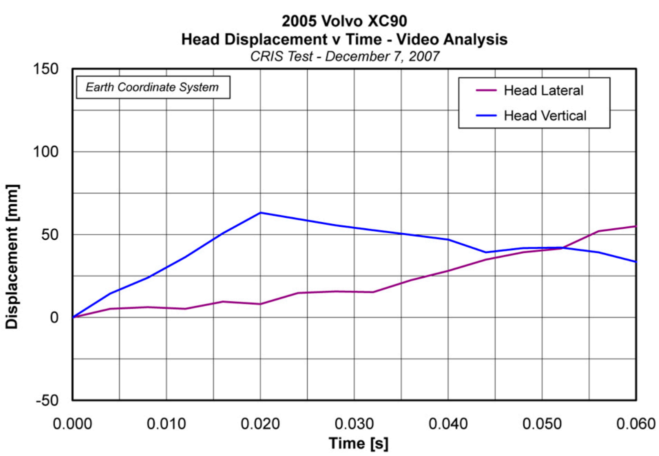

Figure 23: Component displacements of the ATD head in the earth-based reference system.

Recall that the neck loading event peaks at 19.3 ms, which is where the vertical displacement profile in **Figure** 23 plateaus. This vertical displacement profile agrees with the displacement profile from the inertial based displacement profile calculated from the ATD acceleration data (**Figure 16**). The same comparison can be made in the earth-based reference frame for the vertical velocity profiles between the video analysis (**Figure 24**) and the ATD acceleration data (**Figure 17**). These comparisons validate the earlier analysis from an independent data set.

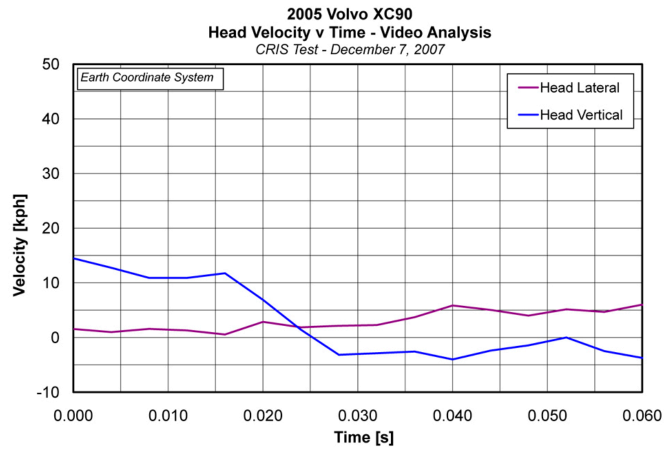

Figure 24: Component velocities of the ATD head in the earth-based reference system.

The video analysis is only sufficient to determine the overall occupant kinematics; it is not suitable to illustrate the mechanism of neck loading during the head impact. The measurements made by the neck load cells and head accelerometers are more appropriate to determine the origin of neck loading during rollover events. In fact, SAE J211 states that the cut-off frequency for both head accelerations and neck loads shall be 1650 Hz, well above the 250 Hertz video data. It is for this reason that the authors encourage the reader to be cautious about the propriety of using video analysis data for determining the timing between ATD neck loading and head kinematics. The video data do provide confirmation that the overall displacements are consistent with the high frequency data analyzed in the earth coordinate system.

ISUZU RODEO TEST – IMPACT 1

A production 1996 Isuzu Rodeo was modified, dynamically balanced, and tested on the CRIS machine. The Rodeo was modified by adding 4130 steel plate at select locations along its left and right roof rails, A-pillars, and B-pillars. Additional modifications included: steel tubes inserted within the A-pillars, the replacement of the original front roof header with one from a Volkswagen Touareg, and the replacement of the original roof bow with one from a Volvo XC90. Finally, voids within the side roof rails, the front header, roof bow, and the B-pillars were filled with an expandable two-part rigid polyurethane foam that had a density of 23 pounds per cubic foot. The initial conditions at impact were: 317 deg/s roll rate, and zero degrees pitch and yaw. The drop height, from release to first contact, was 480 mm. The position of the ATD head and the vehicle at impact was such that the top of its head was adjacent to the interior roof rail between the A- and B-pillars. The driver side window was closed for this test. As with all of the CRIS tests, the vehicle was released from the CRIS fixture and fell to the ground unconstrained. **Figure 25** depicts the vehicle and ATD orientation as the vehicle contacted the ground.

Figure 25: Ground contact with the exterior roof panel in the first impact of the Rodeo CRIS test.

The two plots in **Figure 26** and **Figure 27** represent the lateral and vertical component forces acting on the ATD head in the earth's inertial reference frame. It can be seen that for the lateral components, the total head force is not necessarily larger than the sum of the inertial component and the neck component. This is explained by observing that these forces are not necessarily acting in the same direction. Like the XC90 test, the vertical inertial components of force dominate the total force during a short duration after initial contact, and diminish within approximately 4ms of head contact. However, unlike the XC90 test, these inertial forces do not go to zero. This occurs because once the head comes in contact with the modified roof rail, and the head changes velocity considerably, it continues laterally through the adjacent window opening until it contacts the ground. This can be seen in both the lateral and the vertical directions. It can also be seen that the inertial force is fairly low during the time it takes the head to drop from the roof rail to the ground. Although this impact was considerably different than that of the XC90, the contribution of torso augmentation can clearly be seen in the vertical direction.

It is noteworthy to point out that the second head loading event seen in **Figure 27** is directly with the ground after the head continued passed the roof rail. The loading profile demonstrated similar head inertial and neck force characteristics to that seen in the preceding head contact with the vehicle structure just milliseconds earlier.

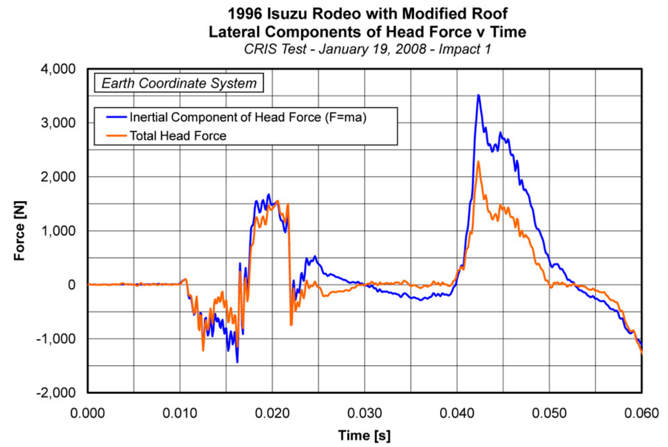

Figure 26: Lateral inertial and total head force during the first Rodeo CRIS impact.

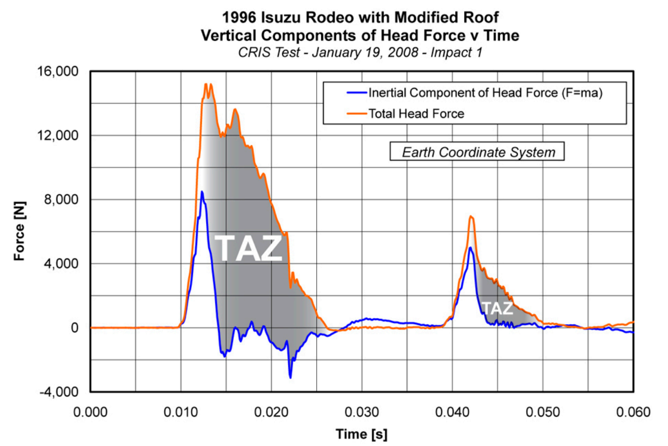

Figure 27: Vertical inertial and total head force during the first Rodeo CRIS impact.

Components of the head velocities and displacements are plotted with the measured neck loads in the earth coordinate system in **Figure 28** and **Figure 29**. Earth-based head displacement and neck load data show that the head is moving toward the ground (vertical direction) and slows considerably once the head contacts the roof rail. It can be seen that as the head continues through the adjacent window opening its vertical velocity comes to a stop only after the head comes in contact with the ground.

These plots also illustrate the large lateral velocity between the ground and the head. The lateral velocity at the outer skin of the roof just prior to it interacting with the ground is also quite large, and it is this difference that imparts a large lateral force to the roof, resulting in a large torque to the vehicle and an increased roll rate.

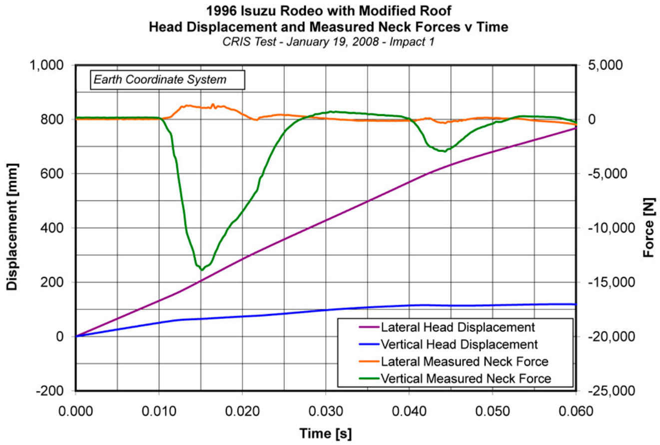

Figure 28: Measured neck loads and head displacements in the earth coordinate system.

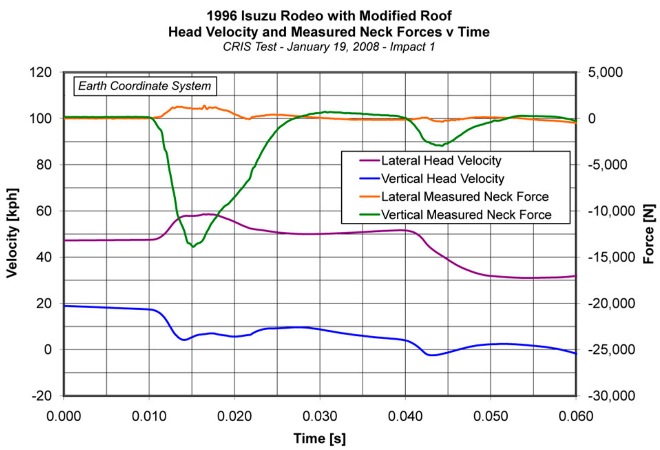

Figure 29: Measured neck loads and head velocities in the earth coordinate system.

The initial lateral and vertical head velocities from the plot in **Figure 29** were 47 kph and 19 kph, respectively. A vector analysis, similar to that done for the XC90 impact, was performed for the first Rodeo impact and is presented in **Figure 30**. Comparison of the vector analysis and the electronic data again demonstrates reasonable agreement.

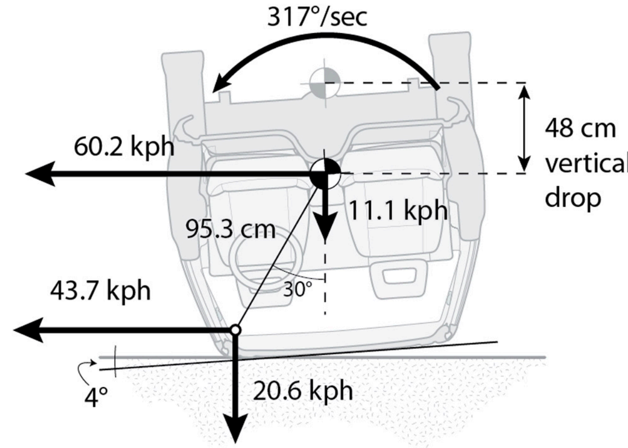

Figure 30: Vector velocity analysis of the first impact in the Rodeo impact in the earth-based reference frame (forward looking aft).

The screen capture from the onboard rear high-speed video camera in the Rodeo test (**Figure 31**) shows the orientation of the ATD with the interior of the left roof rail. The head was not in contact with the roof rail, which is not entirely clear in this image, but is known based on the zero compressive neck load shown in **Figure 29**.

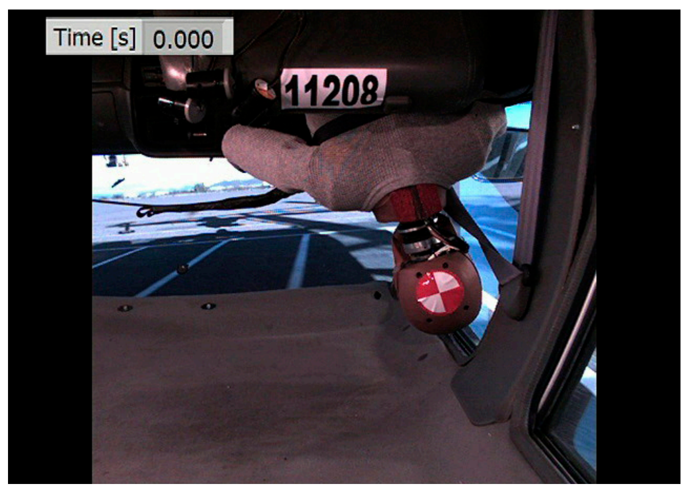

Figure 31: Screen capture of the onboard high-speed video of the driver ATD in the Rodeo CRIS test at vehicle-to-ground contact.

The peak measured compressive neck load occurred at 15.2 ms and the nearest frame in the high-speed video to this peak was at 16 ms, which is shown in **Figure 32**. The physical loading of the neck in compression is clearly observed by comparing the aluminum neck rings at 16 ms versus the unloaded neck at 0 ms. Interestingly, both the XC90 and the Rodeo had ATD head clearance at vehicle contact with the ground. The peak measured neck load occurred earlier in the Rodeo test (15.2 ms) than in the XC90 test (19.3 ms), which is attributable to two things in the Rodeo test: (1) the head was closer to the roof rail and (2) a higher vertical velocity based on the initial conditions. An attempt to apportion the role played by these factors in the timing of the neck load has not been made.

Figure 32: Screen capture of the onboard high-speed video of the driver ATD in the Rodeo CRIS test near peak measured compressive neck load.

As the impact progressed, the closed driver side window fractured at approximately 24 ms, as shown in **Figure 33**, which was after the peak compressive neck load occurred. This indicates that at least within the geometry of the Rodeo's interior, the 50th ATD head is capable of sustaining injurious neck loading by contact with the interior roof rail with the side window intact. It is unclear whether the dynamic deformation of the roof structure or head contact with the glass caused it to fracture.

Figure 33: Screen capture of the onboard high-speed video of the driver ATD in the Rodeo CRIS test at side window fracture.

ATD head movement and deformation to the roof structure were evaluated from the onboard high-speed video camera and is plotted in **Figure 34**. At 16 ms this moving reference frame indicated that the vertical component of the roof was displaced 31 mm closer to the camera, while the head was displaced a minute amount. It was at this instant the head contacted the roof rail. The head then traveled out of the adjacent window opening, and at 32 ms made direct contact with the ground. After that point, the roof and the head were stopped vertically on the ground, and the video analysis indicated that they travelled approximately the same distances.

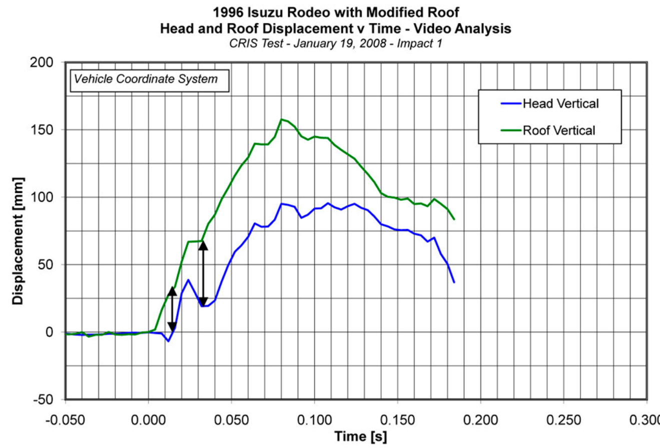

Figure 34: Roof and head displacement calculated from the on-board high-speed video camera. Arrows indicate timing of head-to-roof rail and head-to-ground contact.

The lateral and vertical velocities are illustrated in **Figure 35**, and like the XC90 test, there appears to be a biphasic event associated between their peaks. The vertical component of the velocity occurs first followed by the lateral component.

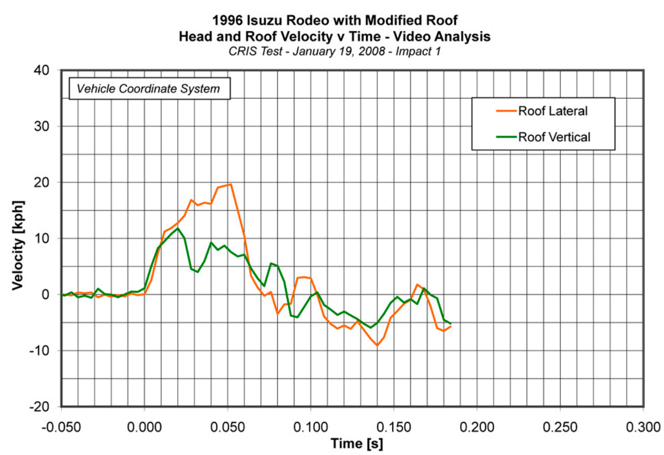

Figure 35: Roof velocity calculated from the on-board high-speed video camera.

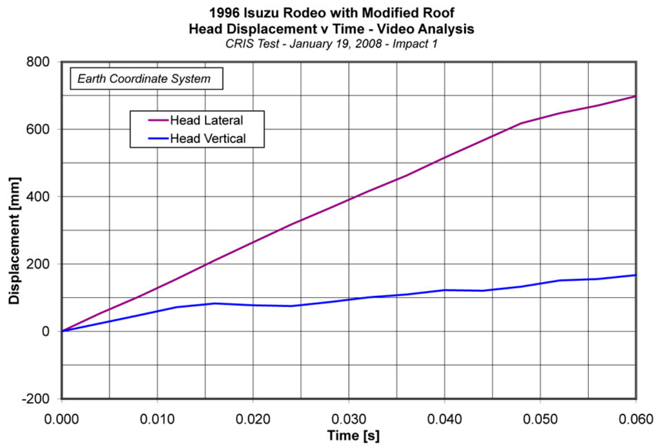

Figure 36: Component displacements of the ATD head in the earth-based reference system.

The components of the head displacements and velocities during the duration of head contact are illustrated in **Figure 36** and **Figure 37**.

It may appear from the data that the vertical head displacement actually continued toward the ground even after contact with it. The data do not suggest that the head penetrates the ground, but when analyzed in conjunction with the video, indicate that the tracked target on the head was actually rotating giving the appearance of additional movement toward the ground. To illustrate this point, a frame from the onboard high-speed video camera was captured at 60 ms and is shown in **Figure 38**.

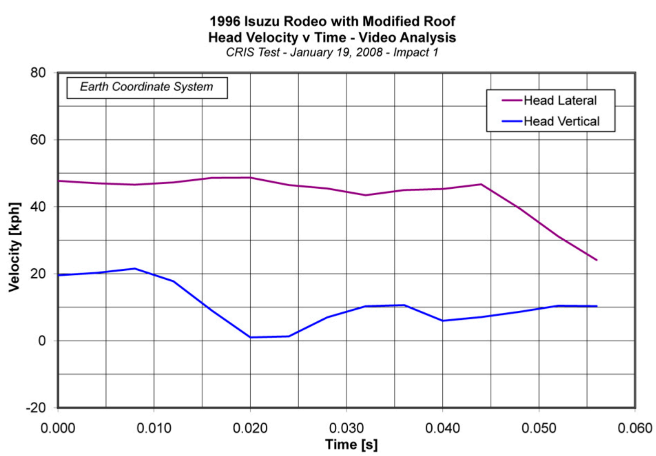

Figure 37: Component velocities of the ATD head in the earth-based reference system.

Figure 38: Video frame captured from the onboard high-speed video camera at 60 ms showing the head rotation after the initial neck loading.

HEAD COORDINATE DATA

Detailed analysis of the XC90 and Rodeo data required a combination of video analysis, electronic data, and several coordinate transformations to determine the mechanism of upper-neck loading. Much of the same information can be seen if the same analysis is simply conducted in the head coordinate system. For the XC90 test, **Figure 39** illustrates the difference between the total head forces calculated in the earth reference frame and total head forces calculated in the head reference frame. The plot shows, particularly in the vertical direction, that the difference between the measured force and the total force performed in the two coordinate systems is minimal.

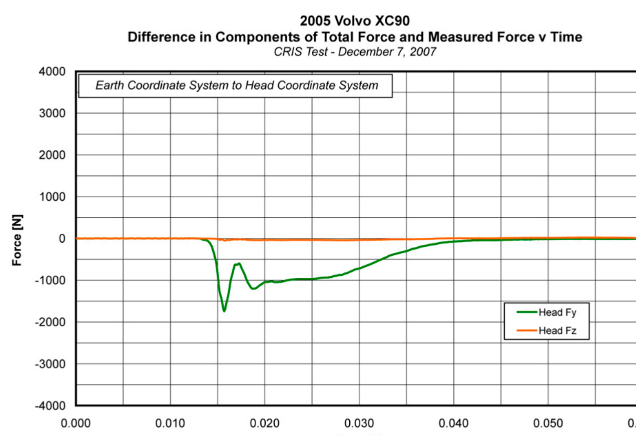

Figure 39: Difference between detailed analyses for the XC90 in the earth reference frame versus the head reference frame.

The same comparison can be made for the head contact during the Rodeo test. **Figure 40** illustrates the difference in forces between the Earth coordinate system and the Head coordinate system for the first roof-to-ground contact. It can be seen that the difference between the vertical components is relatively small, even though the head contact was at the outboard roof rail. The difference in the vertical component only becomes large once the head has passed through the adjacent window opening (**Figure 41**), and the head angle becomes large enough to drive this discrepancy. The results of these comparisons show that for the primary impacts there is little difference between the two coordinate systems, and that for a force analysis in the vertical direction we need only assess the forces in the head coordinate system.

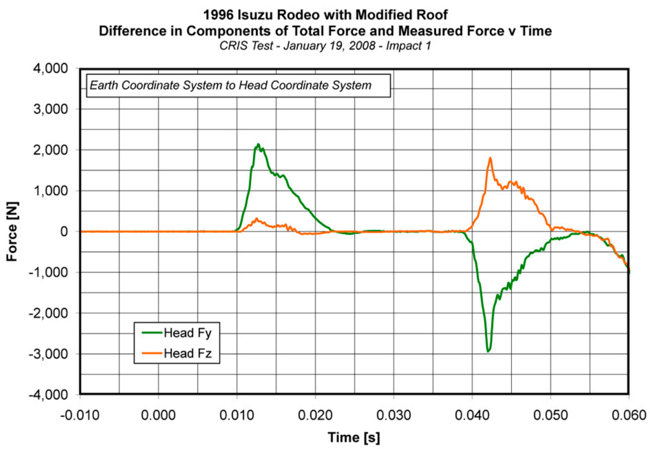

Figure 40: Difference between detailed analyses for the Rodeo in the earth reference frame versus the head reference frame.

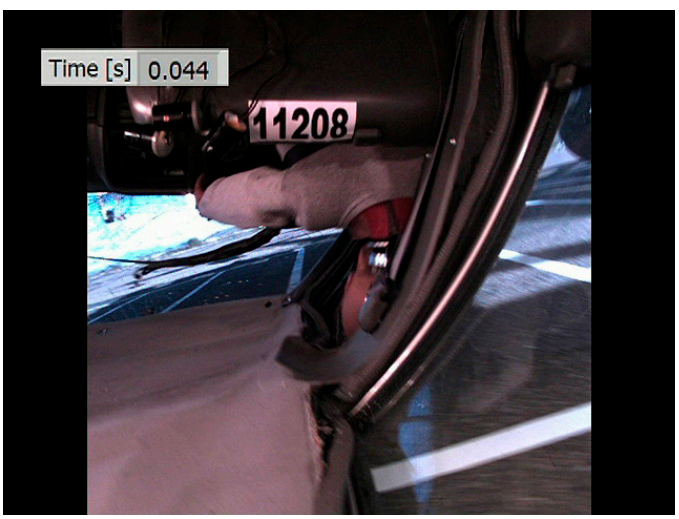

Figure 41: Frame captured from the onboard high-speed video of the Rodeo test showing head-to-ground contact at 44 ms.

Since the vertical head analysis is sufficient to determine the origin of neck loading, a force analysis in the head reference frame is presented in the APPENDIX for all of the head impacts. **Figure 42** through **Figure 47** represent the Crown Victoria CRIS tests, **Figure 48** and **Figure 49** represent the Blazer CRIS tests, **Figure 50** contains the XC90 CRIS test, and the Rodeo CRIS tests are presented in **Figure 51** and **Figure 52**.

DISCUSSION

The critical issue in the authors' rollover inquiry was to understand and illustrate the transient neck loading during a roof-to-ground contact in a rollover. The simple question is whether injurious force applied to the neck is primarily derived from roof crush accelerating the head toward the neck and torso or from the continued motion of the torso being decelerated in part by forces applied through the neck against an already slowed head.

Prior studies have already shown that the supposed downward motion of the roof is only observed from the deceptive accelerated reference frame of a vehicle mounted camera (Moffat et al., 2003, Orlowski et al., 1985). Prior studies have also shown that the roof deformation only becomes significant well after instrumentation demonstrates that the significant neck loading has already occurred (Bahling et al., 1990, James et al., 2007, Moffat et al., 2003, Orlowski et al., 1985). The present study examined the acceleration of the head with respect to an inertial frame in six degree-of-freedom rollover contacts and found that the inertial acceleration of the head had largely already taken place before the significant neck loading occurs. There was fundamentally a three-stage event consisting of head acceleration, neck loading, and roof deformation in that order. In all eleven of these CRIS tests studied, roof crush did not accelerate the head into the neck. The head decelerated, the continued torso motion loaded the neck, and the continued vehicle motion loaded the roof structure to maximum deformation. There was overlap among the three phases but the maxima and the primary events were clearly distinct in time. If roof crush actually produced motion of the head toward the torso, head acceleration with respect to an inertial frame would have been observed during the roof deformation.

In the XC-90 test, head acceleration had taken place within the first 5 milliseconds of head contact. Examination of neck and head forces experienced during the head impact demonstrated that the ATD head was vertically stopped before peak measured neck forces were generated. This occurred because the head was not rigidly coupled to the body and, therefore, its motion was arrested by the roof panel and ground before the torso was stopped. At the time of the first peak, which was dominated by the head deceleration, the force due to the inertial component of the head accounted for approximately 65% of the total force. Continued torso motion loaded the neck in compression, after the head was slowed. The second peak was dominated by decelerating the torso and occurred approximately 3 ms after the initial peak. The pulse duration of the measured neck force (approximately 27 milliseconds) had a much longer duration than the initial head force duration (5 ms). This was consistent with the longer torso stopping distance provided by neck compression compared to the head striking the interior roof panel. The subsequent peak in neck loading created by slowing the torso was a result of the ATD continuing to move into the stopped roof structure. The impulse associated with head acceleration was consistent with that necessary to eliminate the vertical component of the head's momentum. The continued force on the head through the neck did not produce acceleration of the head since the head was in contact with the vertically stopped roof structure.

The head and neck loading profile just described was designated as the Torso Augmentation Zone (TAZ). It is defined as the area between the total head force and the inertial head force. These CRIS tests and the methodology presented in this study clearly outline the origin of neck loading for the given loading conditions. For occupants in real world rollovers with similar loading scenarios, the TAZ represents a plausible basis for neck injury. If ground contact is similar to both reinforced and unreinforced roof structure impacts in producing neck loading, roof deformation can hardly be invoked as the operative mechanism. This point is further illustrated in the Rodeo test by the head and neck load profiles collected during the ATD head impacts that were directly with the ground (two out of three as seen in **Figure 51** and **Figure 52**). The loading profiles in these impacts had the same characteristics as those impacts where the roof structure was present.

During far-side head contacts in rollovers, the head stops vertically and slows laterally. Continued motion of the body loads the neck. Continued motion of the vehicle loads the roof supports, first vertically and then more laterally as the vehicle rotates. Roof deformation is greatest late in the event with more lateral contact. By that time, the neck loading is largely over because the torso by that time is also loading laterally into side structure instead of vertically into the neck. In addition, from an inertial reference frame, the head does not undergo significant acceleration later in the contact since the late lateral roof deformation is derived from the continued motion of the rotating vehicle not in contact with the ground.

CONCLUSION

This paper examines basic principles of rollover kinematics and utilizes actual rollover test data to demonstrate those principles. The data presented in this study demonstrate the timing of head and neck loading as a result of ATD head contact with a vehicle roof during a far-side ground contact. The short-duration head acceleration followed by a longer-duration neck force is similar to a diving impact demonstrated in studies on cervical spine tolerance (Nightingale et al., 1996). In the impacts analyzed and presented in this study, injurious levels of neck compression were a result of torso loading the neck against a head that was vertically stationary.

The findings of this study are consistent with the view that ground contacts of an upper vehicle structure during rollover produce neck injury on the basis of a component of continued torso motion toward a head whose motion has been changed prior to the neck-loading event. Specific conclusions based on the analysis performed on these CRIS tests include:

1. The origin of neck loading events in rollovers must be analyzed from a non-accelerating, non-rotating inertial reference frame.
2. Head accelerometers represent measurements in the inertial reference frame and can be used in appropriate tests to distinguish real from apparent head acceleration.
3. Relevant tests of rollover events must utilize fully unconstrained (six degree-of-freedom) impacts of vehicles with appropriate mass, moments of inertia, and translational and rotational velocities.
4. A typical far-side roof contact can be characterized as a tri-phasic event involving early short duration head acceleration sufficient to eliminate the vertically downward component of head velocity; later, longer duration neck loading derived from a component of continued torso motion without head acceleration; and still later, much longer duration roof deformation which does not yield meaningful head acceleration or injurious neck load.
5. In the tested configurations, roof deformation was a biphasic event consisting of early vertical followed by later lateral components. No meaningful head acceleration continued into either phase.
6. Inertial sensors in the head demonstrate that the bulk of the head acceleration event is over within about 5 milliseconds of head contact for the tested parameters, ending prior to the main neck loading pulse (Torso Augmentation Zone) and well before significant roof deformation.
7. Roof deformation did not accelerate the head into the neck.

ACKNOWLEDGMENTS

The authors would like to acknowledge Ford Motor Company for the funding of Crown Victoria CRIS tests, Isuzu Motors for the funding of the XC90 and the Rodeo CRIS tests, and General Motors for the funding of the Blazer CRIS tests. The analysis presented in this manuscript was conducted independently by the authors and in a collaborative effort to illustrate the fundamentals of rollover dynamics and injurious occupant loading in a rollover.

REFERENCES

1. Ashby, B., Lai, W., Carhart, M., Newberry, W., Weaver, B. and Ford Corrigan, C. (2007) "Compressive Neck Preloading During the Airborne Phase of Vehicle Rollover," Society of Automotive Engineers, No. 2007-01-0377.
2. Bahling, G., Bundorf, R., Kaspzyk, G., Moffat, E., Orlowski, K. and Stocke, J., "Rollover and Drop Tests - The Influence of Roof Strength on Injury Mechanics Using Belted Dummies," Proceedings of the 34th Stapp Car Crash Conference, Orlando, FL, 1990.
3. Bidez, M., Cochran, J. and King, D. (2005) "Roof Crush as a Source of Injury in Rollover Crashes—An Independent Analysis of Autoliv SUV Rollover Tests B190043, B190042, B180220, B180219," March 30, Public Citizen https://www.citizen.org/autosafety/rollover/crashwrth/.
4. Carter, J., Habberstad, J. and Croteau, J. (2002) "A Comparison of the Controlled Rollover Impact System (CRIS) with the J2114 Rollover Dolly," Society of Automotive Engineers, No. 2002-01-0694.
5. Chirwa, E., Mao, M., Chen, T. and Latchford, J., "Flaws in Malibu I and II interpretation of test results that have influenced many poor rollover roof designs," iCrash, Athens, Greece, 2006.
6. Cooper, E., Moffat, E., Curzon, A., Smyth, B. and Orlowski, K. (2001) "Repeatable Dynamic Rollover Test Procedure with Controlled Roof Impact," Society of Automotive Engineers, No. 2001-01-0476.
7. Friedman, D. and Nash, C. (2001) "Advanced Roof Design for Rollover Protection," ESV, No. 01-S12-W-94.
8. Friedman, D. and Nash, C., "Reducing Rollover Occupant Injuries: How and How Soon," 19th International Technical Conference on Enhanced Safety of Vehicle Conference, June 2005.
9. Friedman, D., Nash, C. and Bish, J. (2007) "Observations from Repeatable Dynamic Rollover Tests," iCrash, 12.
10. Gloeckner, D., Bove, R., Croteau, J., Ford Corrigan, C. and Moore, T. (2007) "Timing of Head-to-Vehicle Perimeter Contacts in Rollovers," Society of Automotive Engineers, No. 2007-01-0370.
11. James, M., Allsop, D., Nordhagen, R. and Decker, R. (1997) "Injury Mechanisms and Field Accident Data Analysis in Rollover Accidents," Society of Automotive Engineers, No. 970396.
12. James, M., Nordhagen, R., Schneider, D. and Koh, S. (2007) "Occupant Injury in Rollover Crashes: A Reexamination of Malibu II," Society of Automotive Engineers, No. 2007-01-0369.
13. Moffat, E., Cooper, E., Croteau, J., Orlowski, K., Marth, D. and Carter, J. (2003) "Matched-Pair Rollover Impacts of Rollcaged and Production Roof Cars Using the Controlled Rollover Impact System (CRIS)," Society of Automotive Engineers, No. 2003-01-0172.
14. Moffatt, E. A. and James, M. B., "Headroom, Roof Crush, and Belted Excursion in Rollovers," Society of Automotive Engineers, 2005.
15. Nightingale, R., McElhaney, J., Richardson, W. and Myers, B. (1996) "Dynamic Responses of the Head and Cervical Spine to Axial Impact Loading," Journal of Biomechanics, 29.
16. Orlowski, K., Bundorf, R. and Moffat, E. (1985) "Rollover crash tests—The influence of roof strength on injury mechanisms," Society of Automotive Engineers, No. 851734.
17. Strother, C., Smith, G., James, M. and Warner, C. (1984) "Injury and Intrusion in Side Impacts and Rollovers," Society of Automotive Engineers, No. 840403.
18. Yamaguchi, G., Ashby, B., Luepke, P., Moore, T., Bove, R. and Ford Corrigan, C. (2007) "Theoretical Analysis of a Method of Computing Dynamic Roof Crush During Rollovers," Society of Automotive Engineers, No. 2007-01-0366.
19. Serway R: Physics for Scientists and Engineers with Modern Physics, 4th, Fort Worth, Saunders College; 1996.
20. Nightingale R, McElhaney J, Richardson W, Myers B: Dynamic Responses of the Head and Cervical Spine to Axial Impact Loading, *Journal of Biomechanics*, 29(3), 307-18,1996.

APPENDIX

The following plots in this appendix present the head forces in only the vertical direction within the head reference frame. The measured head accelerations were made relative to the earth's inertial reference frame but oriented within the head coordinate system. The measured neck forces and calculated forces presented below are oriented within the head coordinate system. Since the ATD coordinate system during these CRIS impacts were nearly aligned with the earth's reference frame (that is there was a small angle between the head coordinate system and the earth's inertial coordinate system), the forces on the ATD head within the head coordinate system was sufficient to illustrate the origin of neck loading.

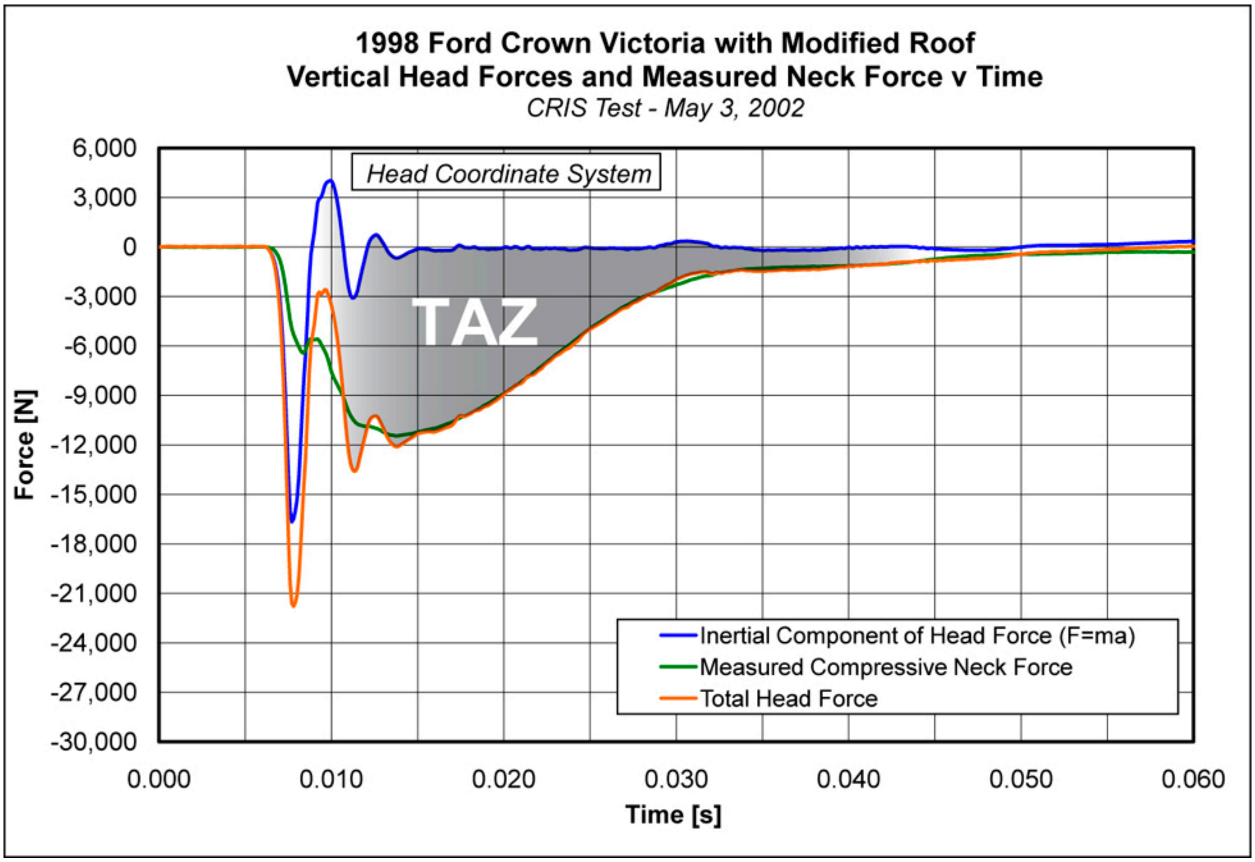

Figure 42: Vertical head forces and measured neck forces in the head coordinate reference frame.

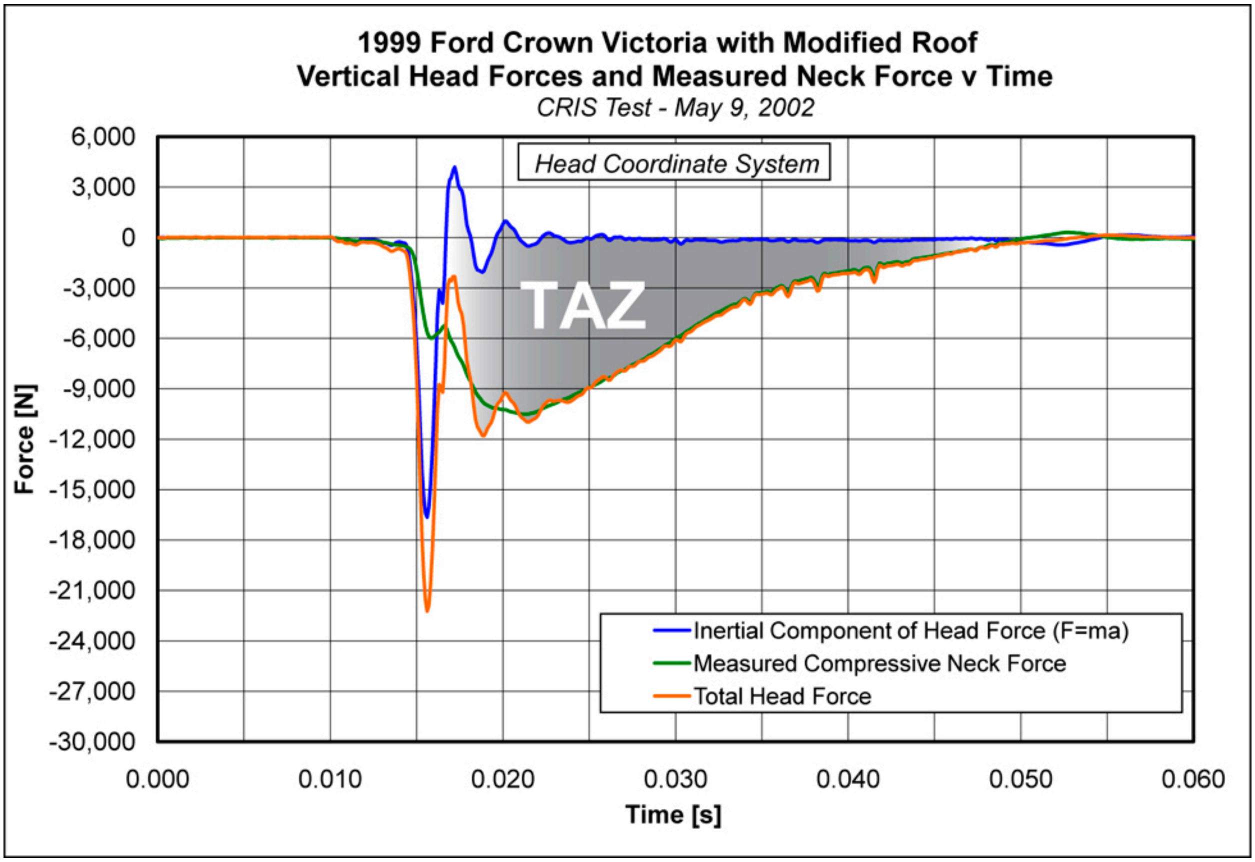

Figure 43: Vertical head forces and measured neck forces in the head coordinate reference frame.

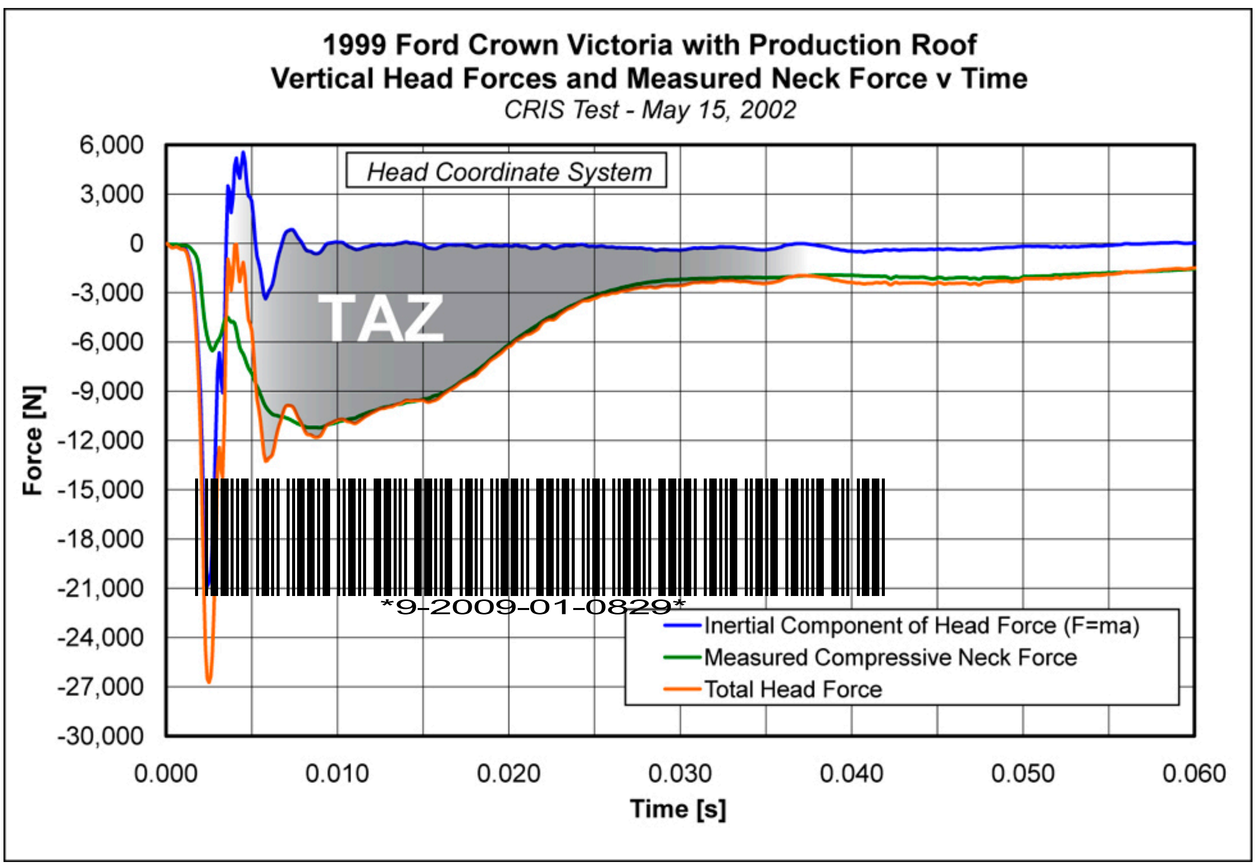

9-2009-01-0829

Figure 44: Vertical head forces and measured neck forces in the head coordinate reference frame.

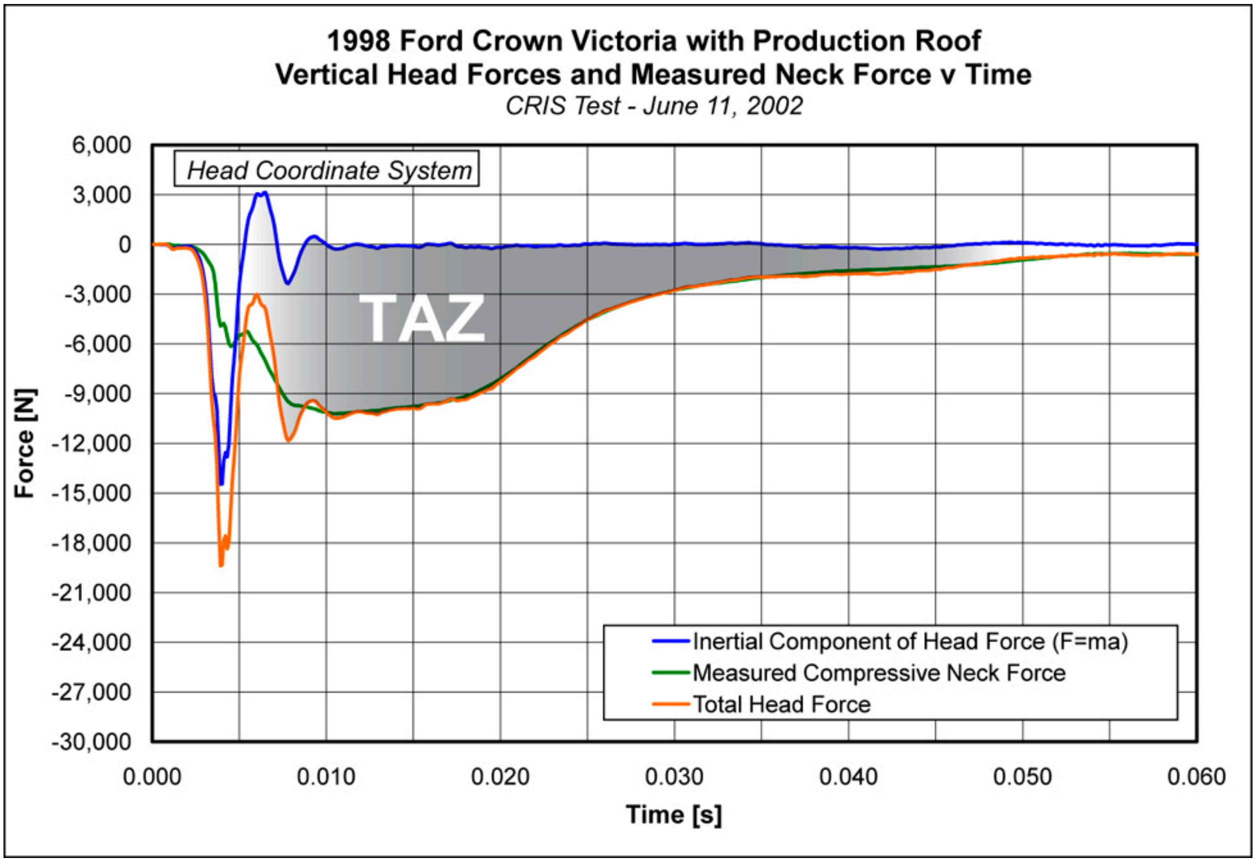

Figure 45: Vertical head forces and measured neck forces in the head coordinate reference frame.

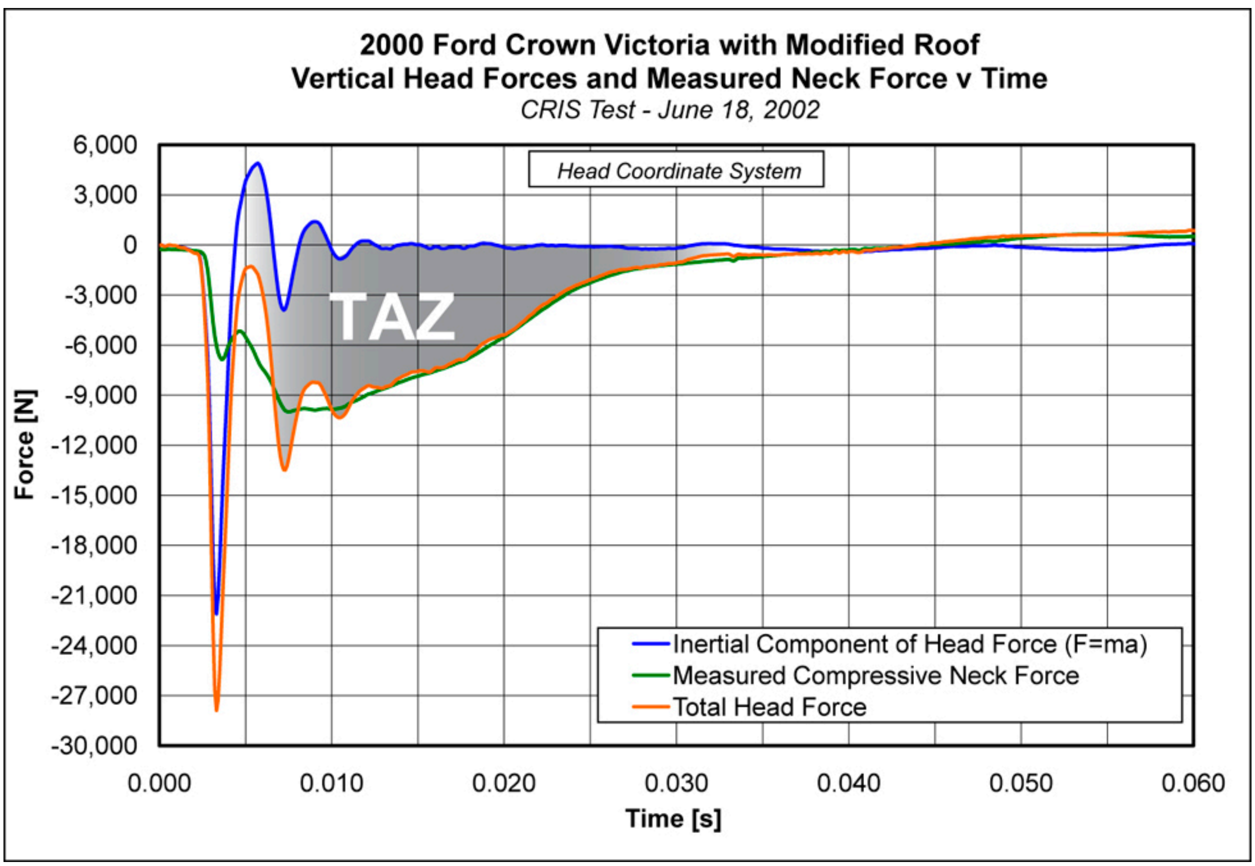

Figure 46: Vertical head forces and measured neck forces in the head coordinate reference frame.

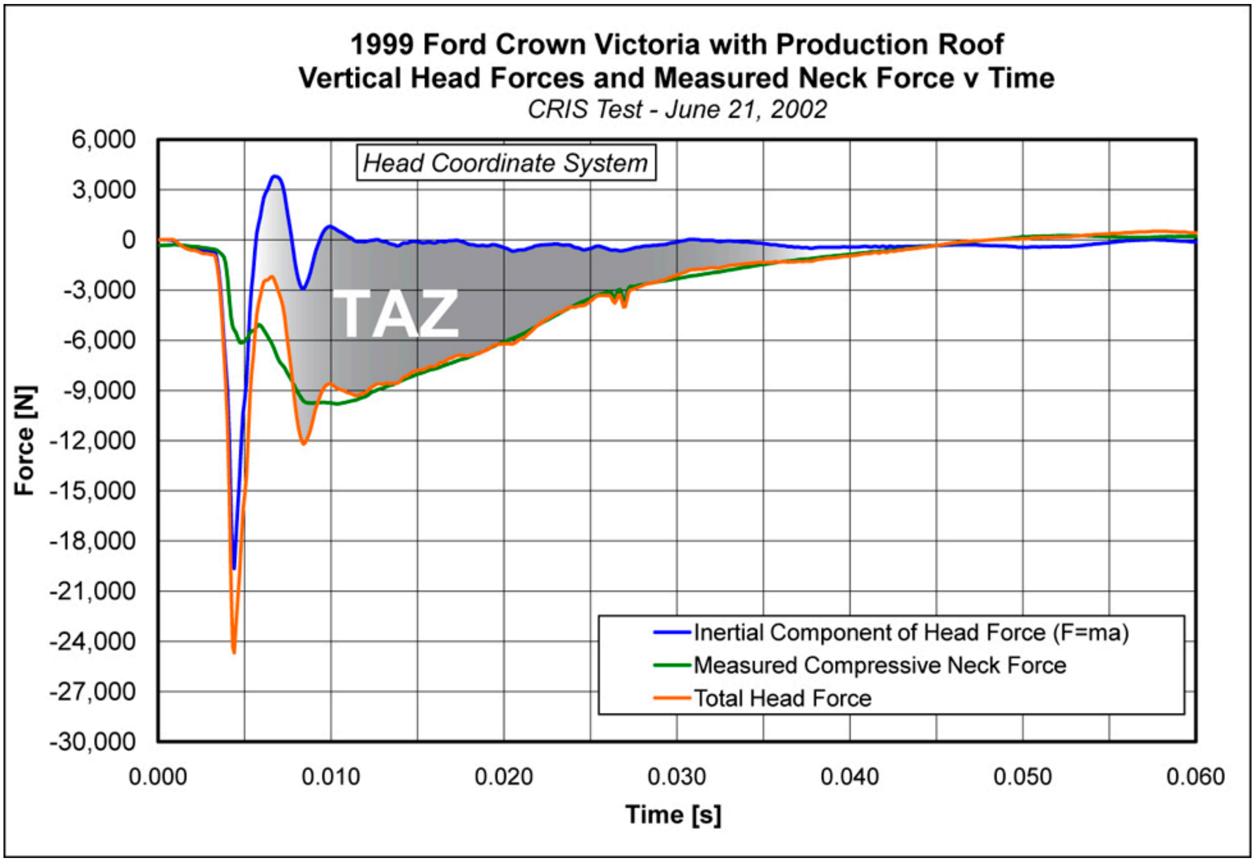

Figure 47: Vertical head forces and measured neck forces in the head coordinate reference frame.

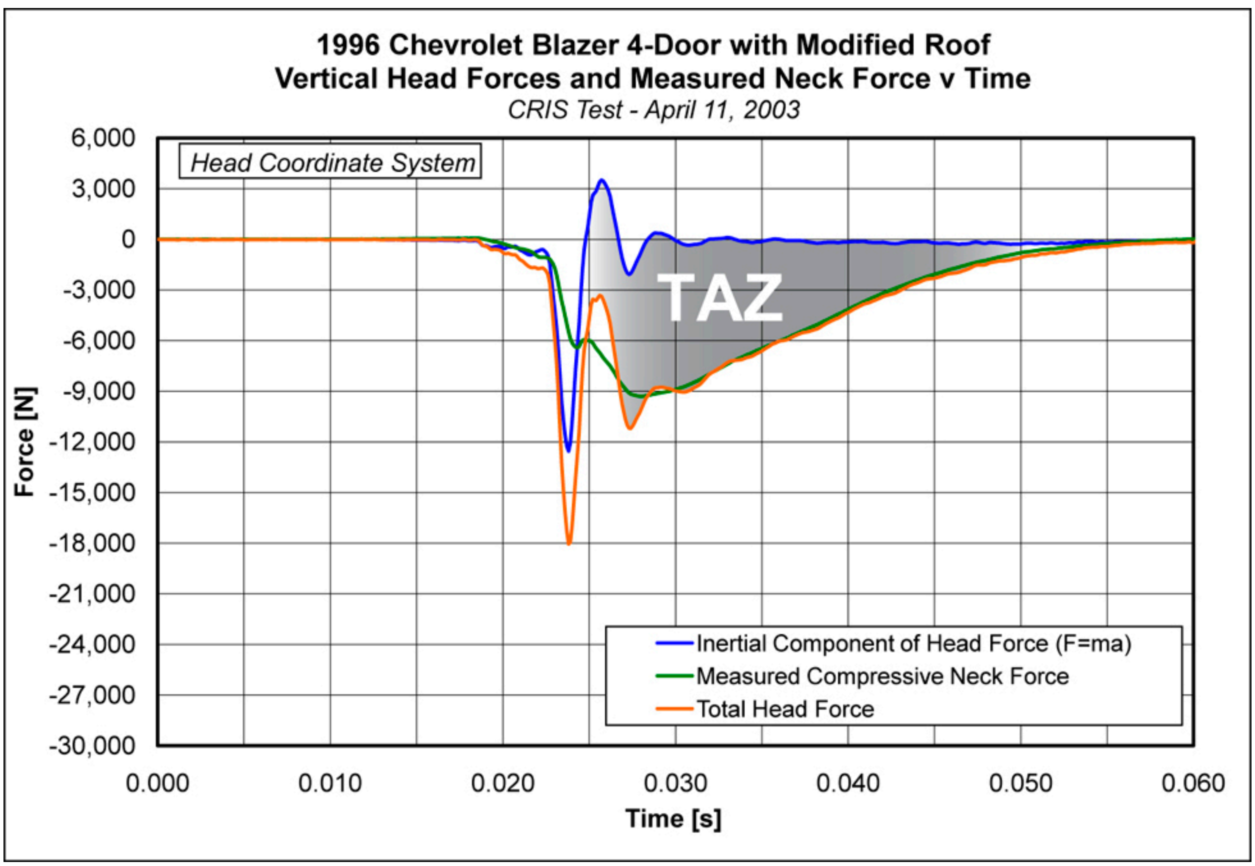

Figure 48: Vertical head forces and measured neck forces in the head coordinate reference frame.

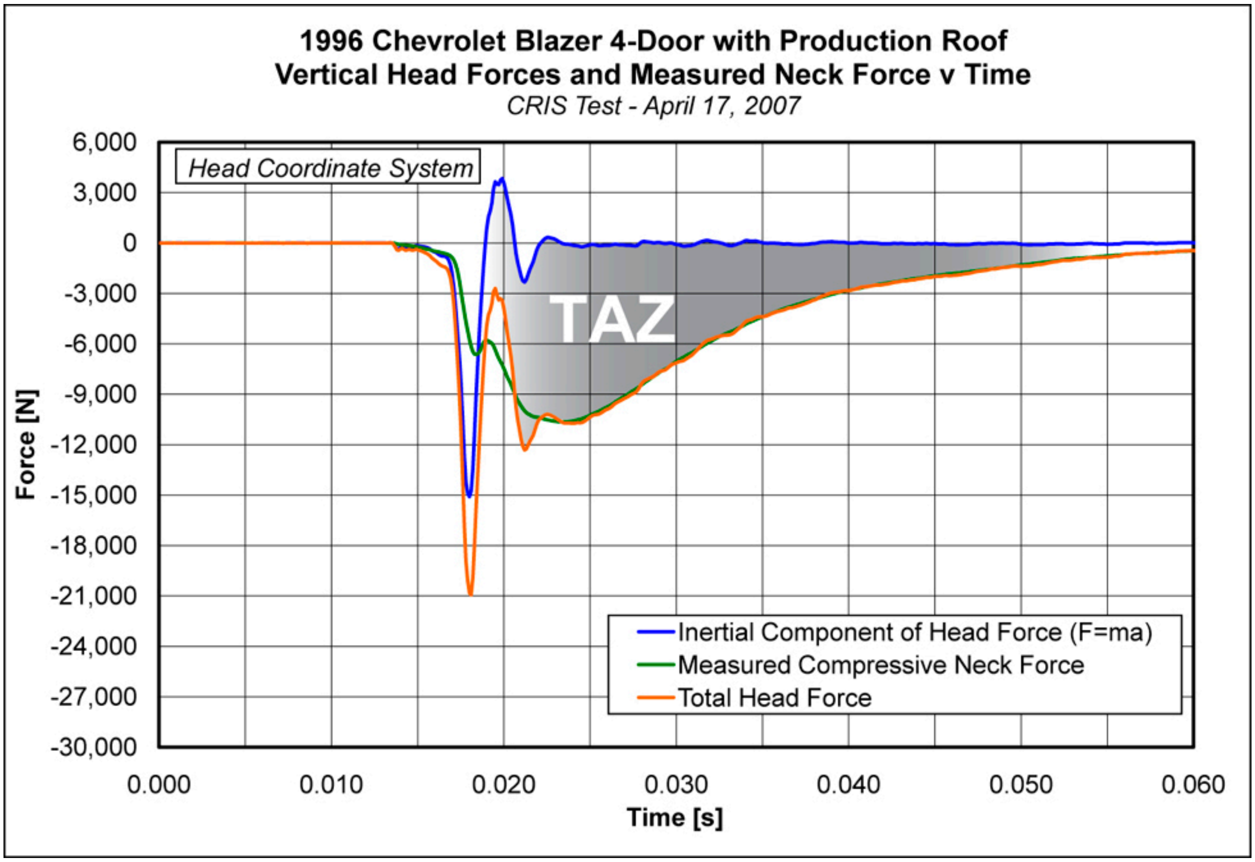

Figure 49: Vertical head forces and measured neck forces in the head coordinate reference frame.

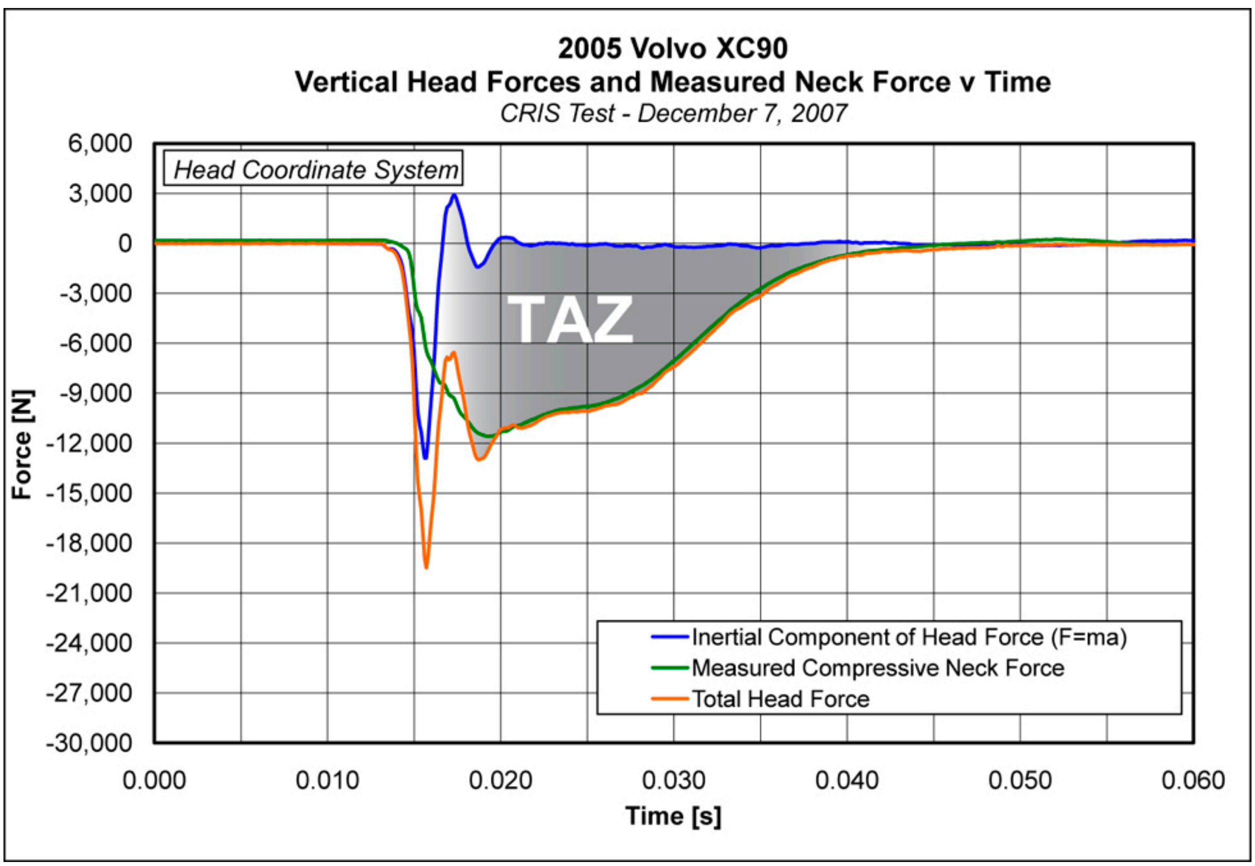

Figure 50: Vertical head forces and measured neck forces in the head coordinate reference frame.

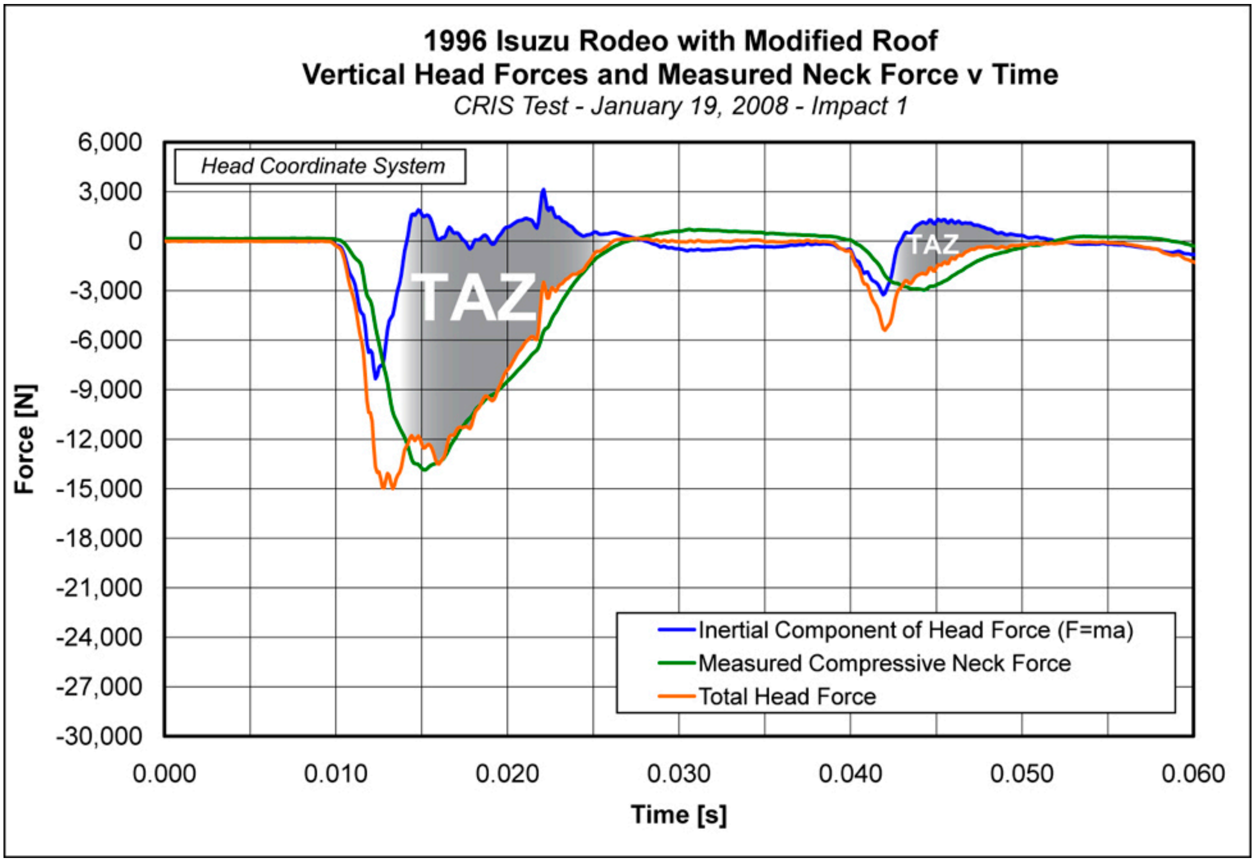

Figure 51: Vertical head forces and measured neck forces in the head coordinate reference frame.

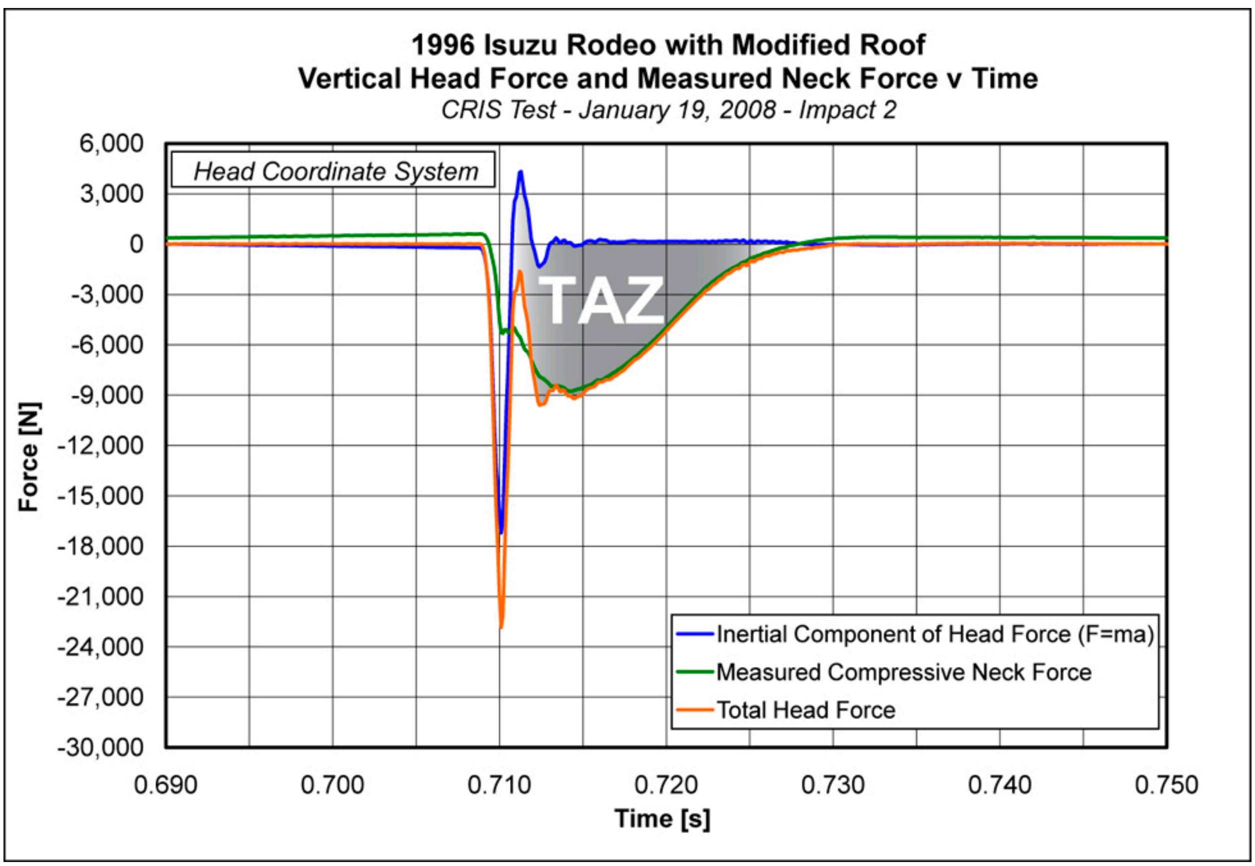

Figure 52: Vertical head forces and measured neck forces in the head coordinate reference frame.